Applied Thermal Engineering 208 (2022) 118167

Contents lists available at ScienceDirect

Applied Thermal Engineering

journal homepage: www.elsevier.com/locate/ate

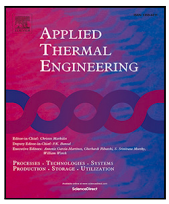

Research paper

Analysis of spray/wall impingement using an ECN single-hole injector and a controlled-temperature wall under realistic engine conditions

Jesús E. Peraza [a], Raul Payri [b], Jaime Gimeno [b,*], César Carvallo [b]

[a] Submer Technologies SL, 08908 L'Hospitalet de Llobregat, Spain
[b] CMT - Motores Térmicos, Universitat Politècnica de València, 46022, Valencia, Spain

ARTICLE INFO

Keywords:
Spray–wall interaction
Post-impingement characteristics
Engine Combustion Network
Lift-off length
Ignition delay
Flame/wall heat flux

ABSTRACT

Spray–wall interactions (SWI) directly affect fuel–air mixture and emissions formation. Therefore, they are considered among the most critical physical processes in engine research nowadays. However, the physics of the wall film formation, propagation, and breakup is not fully understood yet. This work aims to use a thermoregulated steel wall to study the spray–wall interaction phenomenon and its influence on the macroscopic spray behavior. A single-hole injector known as "Spray D" in the Engine Combustion Network was used. n-Dodecane was employed as fuel and the wall has been positioned in four different configurations, varying angle and distance respect to the injector tip. For this work, not only diesel combustion is reproduced in the test rig due to ambient gas engine-like thermodynamic conditions, but wall temperature has been controlled to emulate characteristic values that could be found in the piston of an internal combustion engine. This implies that the spray–wall heat transfer is simulated and its effects on ignition and spray development can be analyzed. Heat flux was measured by employing high-speed thermocouples fitted in the wall and by the use of an one-dimensional transient wall heat model. Three high speed cameras were simultaneously used to observe the SWI, one for the Schlieren optical technique which allows to study the vapor phase of the spray and to determine the ignition delay, another one to observe the natural luminosity of the flame, and finally, an intensified camera was used to determine the lift-off length by observing the chemiluminescence of the OH*. An interesting finding obtained in this work was a boundary layer formation due to the thermal diffusion that contributes to cool down the spray and to delay the high-temperature chemical reactions. Results show a substantial increment of the heat flux and the wall temperature variation with both ambient temperature and density by increasing the flame temperature and gas entrainment. The exposure to the cold wall affects the ignition delay variation with the injection pressure and the wall distance. It was found that the wall temperature (in the range of tested conditions) did not affect the lift-off length location.

1. Introduction

The concern of the international community regarding the protection of the environment is increasingly growing. Due to this, governments have decided to create rigorous emissions regulations, forcing different manufacturers and researchers to find alternatives to design more efficient, cleaner, and economically accessible engines. In the field of engine research, efforts using computational and experimental approaches are applied together to achieve this common goal. Therefore, in recent years a substantial understanding of the phenomenon of fuel injection, spray development, and the combustion process in engines has been achieved [1–3]. However, following the trends of continuous improvement and creation of more detailed models, there are aspects of the fuel injection process, more specifically, of the spray–wall interaction that have yet to be understood and improved. The influence of the spray–wall interaction on combustion is quite complex, after impingement a fuel film can form on the walls increasing the unburned hydrocarbons and the soot formation. Additionally, the efficiency of the engine is reduced due to the heat transfer that occurs between the fuel deposits and the walls in the cylinder. On one hand, it is known that the secondary atomization produced by the spray–wall impact promotes the breakup of the droplets, reducing their size, accelerating the evaporation and the combustion process, while on the contrary, the dispersion of the spray in the wall reduces the local spray temperature and may delay ignition. This phenomenon is key especially for direct injection engines under cold start conditions, where low densities and temperatures promote a large liquid spray penetration that might reach the piston and the walls of the combustion chamber.

* Corresponding author.
E-mail address: jaigigar@mot.upv.es (J. Gimeno).

https://doi.org/10.1016/j.applthermaleng.2022.118167
Received 21 October 2021; Received in revised form 23 December 2021; Accepted 2 February 2022
Available online 19 February 2022

Nomenclature

Acronyms

ASOE	After start of energizing
ASOI	After start of injection
CMOS	Complementary metal–oxide–semiconductor
CMT	Centro Motores Térmicos
CWL	Center wave length
ECN	Engine Combustion Network
FDM	Finite differences method
hPhTC	High-pressure high-temperature facility
ICCD	Intensified charge-coupled device
ID	Ignition delay
LED	Light-emitting diode
LoL	Lift-off length
nC12	n-Dodecane (abbr. used in plot legends)
NL	Natural luminosity
SOI	Start of injection
SWI	Spray–wall interaction
TC0	Standard k-type thermocouple
TC1-TC2	Fast-response temperature sensors
TRI-Wall	Thermoregulated and instrumented wall

Greek Symbols

α_w	Thermal diffusivity
ϕ	Spray angle
ρ	Density
τ_w	Start of spray-wall interaction
θ_w	Angle (of the wall)
δc	Boundary layer thickness
Δp	Pressure difference
Δt	Temporal gap
ΔT_w	Variation of wall temperature
ΔX_f	Flame-wall horizontal width
Δz	Variation of wall depth

Subscripts

+	Wall upwards direction
amb	Ambient condition
rail	In-rail, of injection (pressure)
thXX	Measuring point location (in mm)
w	Related to the wall

Variables

$\dot{q}$	Heat flux
p	Pressure
xO_2	Concentration of oxygen
d_{gc}	Distance from geometric center of the wall
d	Distance
k-factor	Conicity factor used in industry
k	Heat conduction coefficient
Re	Reynolds number
R	R-parameter
S	Penetration
T	Temperature
t	Time
X	Horizontal spray spreading
Y	Upwards spray spreading
Z	Spray thickness or height
Fo	Fourier number

Several authors [4–6] have classified the analysis of the spray–wall interaction according to the morphology of the colliding fluid, while other authors [7,8] have contributed to understand the influence of a large number of variables that take place in this phenomenon, as are the properties of the fluid and the surface, and the drops and deposit formation.

Additionally, computational fluid dynamics simulations represent a tool that allows the study of this phenomenon without the need to assess the engine by using experimental techniques. One of the first models of spray–wall interaction was made by Naber and Reitz in 1988 [9], by the using of three different models of behavior: stick or adhesion, reflect or specular rebound, and jet or tangential incidence. Being a relevant work in this matter that gave place to the development of more modern and complex computational works, [10–12].

In the present work, the spray morphology and the spray spreading along the wall are discussed, also aspects regarding the combustion process are addressed. For that, concepts as spray penetration, the lift-off length, and the ignition delay needs to be introduced because they are among the most studied variables in the engine combustion field. The spray penetration is defined as the distance that a spray travels into its medium. Due to its direct relationship with the spray distribution within the chamber and with its suitability as a quality indicator of air–fuel mixture and evaporation, it is one of the most widely studied metrics in spray diagnostics [13–15]. As well, regarding diffusive combustion, as long as the fuel and oxygen are supplied to the flame, the flame front is self-sustained [16,17] and, if the injection duration allows it, the flame can achieve a quasi-stationary structure. One of the most generally accepted models for diffusion flames has been presented by the comprehensive study of Dec [18]. Due to the high jet speed at the nozzle outlet, the flame is “lifted” a determined distance (known as lift-off length or LoL) in respect of the injector tip, having a first liquid and non-reacting zone. Lastly, the ignition delay is defined as the period from the start of the injection up to the instant where induced physical conditions in the air-fuel mixture are compliant to start the combustion. This delay has been widely studied and has shown to be highly dependent on numerous parameters such as ambient temperature and density [19,20], nozzle diameter [20,21] and rail pressure [22,23].

Soot luminosity is predominant in direct flame visualization on a wide range of visible wavelengths respect to other combustion products. However, its formation not only takes time but also its concentration is not uniformly representative for diesel flames stabilization. According to [24] OH* radicals chemiluminescence takes place at the stable flame length, under high-temperature conditions, making them more suitable to measure the lift-off length (*LoL*).

Even when the analysis of free-jet injection and combustion has proven to be exceptionally useful to reach a better understanding on the functioning of injection systems in engine applications and, for the development of accurate empiric and CFD models, it is still a simplistic model of the injection process into a combustion chamber of a reciprocating engine. Spray–wall interaction has a fundamental role in the fuel atomization, mixing and in both combustion behavior and pollutant emissions formation. On the one hand, the incidence and accumulation of fuel in the cylinder walls can lead to the formation of a fuel film that worsens combustion, promotes the emission of carbon monoxide and unburned hydrocarbons and involves energy losses due to the increase of heat transfer. This heat flux from the flame to the

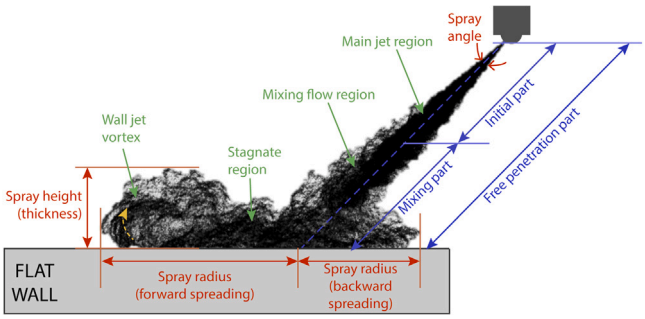

Fig. 1. Model of a diesel impinging spray against a flat wall.

wall is also expected to reduce the spray temperature which could delay the ignition process. On the other side, the impact of the spray with a surface gives place to a secondary atomization produced by the impact and also to a larger exposure of the jet surface to the chamber gases, improving the air–fuel mixing which is well-known to enhance combustion. All those elusive effects on internal combustion engines performance, together with its broad technical applications in other fields such as spray-induced cooling, painting and prevention of solid depositions; make spray–wall interaction to remain nowadays as an active area of research.

Regarding the spray wall interaction phenomenon, not only piston diameters and bore-to-stroke ratios [25,26] have shown to impact the heat losses to metallic walls, but also variations respect to conventional piston bowl geometries are used to isolate sprays or to split the spray between the bowl and the squish region and affect the fuel spreading and soot formation. However, many researches still agree on the need of more basic understanding on spray–wall interaction and further improvements in diesel engine CFD modeling, to predict tendencies on engines performance [26,27]. In spite of the existence of research on soot production under SWI conditions, some of their results are still ambiguous and a conclusive understanding might miss. For instance, the study of [28] presents how the insertion of a wall increases soot formation, specially when it is placed near to the injector. On the other hand, [29] found in the use of SWI respect to free-jet, the potential to reduce or even eliminate soot formation, by means of the increased fuel–air mixing rate and the wall-jet-cooling effect provoked by SWI.

Several works have tried to define the macroscopic characteristics of an impinging spray and its different regions with a general agreement. An adaptation of some of those conceptual models are shown in Fig. 1.

The conditions studied throughout this work, as well as the phenomena and variables analyzed, are intended to widen the fundamental understanding on the spray–wall interaction and to serve as database for model tuning. A real injector known in the Engine Combustion Network as “SprayD” has been used in a range of realistic in-cylinder conditions of high-pressure and high temperature. Nonetheless, the wall has been simplified to be a flat plate in order to insulate the studied phenomenon and extract as much information as possible about the influence of the ambient, injection and wall-positioning conditions in terms of air–fuel mixture, spreading along the surface, combustion parameters and spray–wall heat exchange.

2. Materials and methods

2.1. Visualization chamber and injection system

The experimental campaign was carried out in a high-pressure and high-temperature test rig (hPhTC) present at the research institute CMT - Motores Termicos. This vessel is a constant pressure and flow test chamber that have three optical accesses of 128 mm diameter and allows to reach diesel engine-like thermodynamic conditions. This facility has

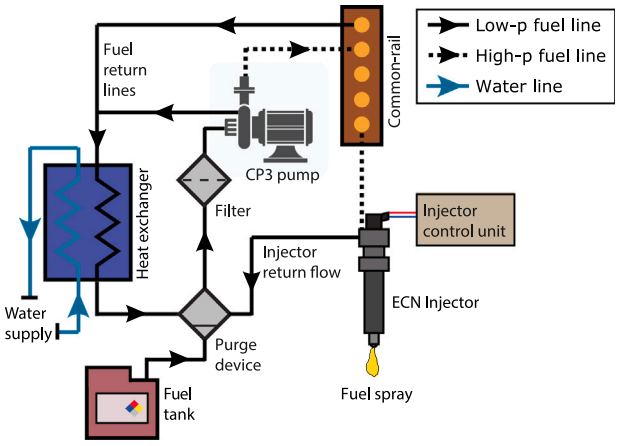

Fig. 2. Scheme of the high-pressure injection system.

been used and described previously in some researches [23,30,31]. The facility allows to work at different oxygen concentration which are monitored using a lambda sensor and at different ambient temperatures using a 30 kW electric heater located right in the entry of the vessel. The chamber has a test section of 200 mm and is not only able to reach chamber conditions up to 1000 K and 13 MPa but also has the capability of providing quiescent and steady thermodynamic conditions, which enables continuous and repeated observation at a wide range of conditions.

For the present work, the possibility of a frontal view has been sacrificed in order to use a conductive metallic wall provided with fast-response probes to register the wall temperature instantaneously during the injection event. The wall was designed as a thermo-well in order to set its surface temperature by gas convection, and it will be described in the following sections..

An axial single-hole Bosch 3–22 injector known as “Spray D” by the Engine Combustion Network (ECN) was used in this work [32]. Its size has been specified to resemble characteristics of heavy-duty diesel injectors with an outlet diameter of 190 μm. Spray D has been specified with a convergent nozzle with a hydro-eroded inlet to suppress the cavitation phenomenon in its inner flow. The geometry and features of this injector have been measured and extensively characterized by several authors [33–35]. Some of those characteristics are gathered in the ECN webpage [32].

The injection setup consist of a standard common-rail system which is mainly formed by a common-rail of 22 cc volume with a pressure regulator controlled by a proportional–integral–derivative (PID) and a Bosch CP3 pump powered by an electric motor. The injector tip was kept at 363 K by using a purpose-made injector holder and an ethylene glycol flow at a constant temperature [15]. This setup is shown in Fig. 2.

2.2. Test matrix

Almost all the test conditions used in the experimental campaign are of common interest to the ECN research group and can be seen in Table 1. Several variations of injection pressures, ambient gas temperatures, wall distances, wall angles, and wall surface temperatures were set, while n-dodecane was employed as injected fuel.

In Table 1 the controlled conditions for the 108 points of the experimental campaign are shown and also can be found the position of the different thermocouples used to measure the temperature changes in the thermoregulated and instrumented wall (referred to hereinafter as TRI-Wall) surface during the injection event.

Regarding the data acquisition, 10 repetitions were made for each condition tested in the experimental campaign and the time between

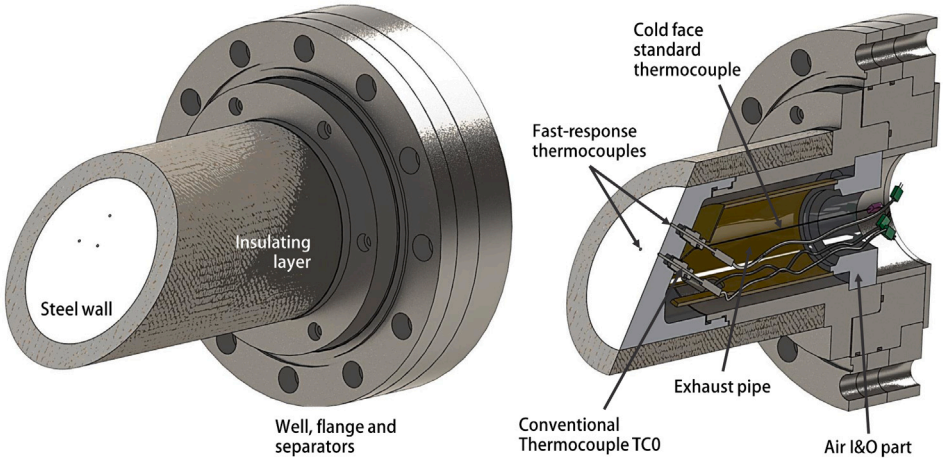

Fig. 3. Thermo-well assembly (d_w = 50 mm; θ_w = 60°). Left: Isometric view. Right: Isometric view with section cut.

Table 1
Test plan for experiments in the TRI-Wall.

Variable	Values	Units
Fuel	n-dodecane	–
Injector	Bosch 3-22 ECN Spray D	–
Energizing time (ET)	2.5	ms
Tip temperature (T_{tip})	363	K
Oxygen fraction (xO_2)	≈0.21	–
Gas temperature (T_{amb})	800–900[a]	K
Gas density (ρ_{amb})	22.8–35	kg/m^3
Injection pressure (p_{rail})	50–100–150	MPa
Wall distance (d_w)	30–50	mm
Wall angle (θ_w)	60–90	°
Wall surface temperature (T_w)	480[a]–550	K
Total test points	108	Points
Thermocouples location[b] (θ_w = 60°)	TC0: d_{gc} = 10 (inline) TC1: d_{gc} = 30 (inline) TC2: d_{gc} = 18 (located next to TC0)	mm mm mm
Thermocouples location[b] (θ_w = 90°)	TC0: d_{gc} = 0 (centered) TC1: d_{gc} = 15 (on the side) TC2: d_{gc} = 20 (inline)	mm mm mm

[a]These conditions were not tested simultaneously.
[b]Please refer to Fig. 4.

each injection event was set to 4000 ms to reestablish the wall temperature to the same target value before the spray–wall interaction occurs.

2.3. Thermo-regulated and instrumented wall system

Fig. 3-left shows the thermoregulated wall with an insulating layer attached to the supporting system used to fix the entire assembly inside the hPhTC. Fig. 3-right shown the thermocouples and the cavity used to cool down the wall surface temperature by gas convection to reach the target condition. The steel wall has a 94 mm diameter and 20 mm of thickness with a fixed inclination angle, each angle is related to a different exchangeable steel wall body, as shown in Fig. 4. Depending on the target distance between the injector tip and the wall, a determined exchangeable separator ring is used. Three thermocouples were used to register the wall temperature variation during the injection event: two fast-response sensors and a standard K-type one.

The internal cavity (thermo-well) is used to keep the wall at a controlled temperature which could be in the range of 430 K and 600 K while the air of the surroundings is hotter.

In Fig. 4 the location of the thermocouples for both wall configurations can be seen, TC0 is always referring to a standard K-type surface thermocouple with a conventional acquisition rate to have a robust reference sensor, while TC1 and TC2 are the names of the fast-response sensors used to acquire the temperature of the wall at a microsecond time-scale.

Before using the thermocouples mounted in the wall, a Fluke temperature bath system was used to calibrate them. The methodology was to expose the thermocouples to a dry bath into aluminum oxide sand fluidized by low pressure air.

2.4. Experimental optical techniques

For the experimental campaign, three cameras were used at the same time to obtain the spray images using different optical techniques with its light main trajectory represented in dashed lines of different colors in Fig. 5. The first camera for the Schlieren imaging (yellow) has been used for the visualization of the vapor phase of the spray and the burned gases produced in combustion. The second camera has been employed to apply the OH* chemiluminescence technique (blue lines) to estimate the flame lift-off length location by observing the light emitted by the OH* radicals. The last camera was used to observe the natural luminosity of the flame through natural luminosity diagnostics (NL) (red lines).

In the case of Schlieren imaging, a continuous Xe-Arc lamp was used as light source. Light then travels to a parabolic mirror that collimates the rays that go through the chamber. Those rays are collected by a UV biconvex lens and a dichroic beam-splitter that let the visible rays pass through it to the Photron SA5 camera while the UV rays are reflected to the intensified Andor iStar camera. In the chamber, density gradients affect refraction index and deviate the rays from their parallel original path that makes that those deviated beams not to reach the camera due to the narrow diaphragm gap.

The camera used to record the natural luminosity has been configured with a long shutter time in order to detect flame regions with low intensity and precursor chemical reactions at the beginning of the exothermic processes that lead to combustion, however, a bandpass filter has been used in order to avoid image intensity saturation. Finally, an ICCD Andor iStar camera, fitted with a 100 mm f/2.8 UV lens and a 310 ±5 nm CWL filter was employed to capture a single image by each injection event. This image is taken only in a time gap during the steady part of the combustion, in order to reduce rep-to-rep deviations. More details about the setup of the optical arrangement can be found in Table 2.

2.5. Image processing and contour analysis

The image processing methodologies are based on strategies to segment the spray and the background using an algorithm that has been internally developed and employed in several works [20,36,37].

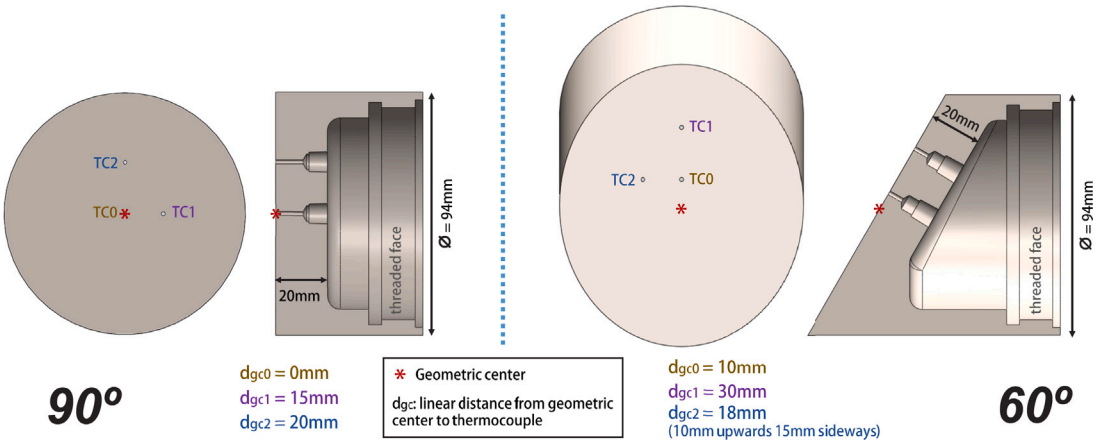

Fig. 4. Wall pieces in normal-to-wall and lateral views. Left: θ_w = 90°. Right: θ_w = 60°. Wall has been simplified being shown without fins nor threads.

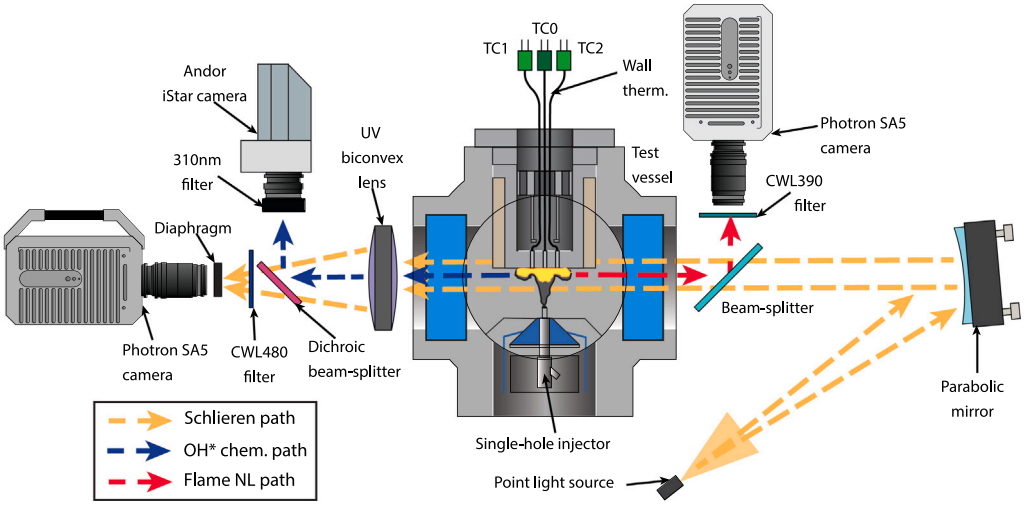

Fig. 5. Optical arrangement employed in the experiments. Schlieren imaging, OH* chemiluminescence and natural luminosity have been simultaneously used. Dashed lines indicate the main light path for each technique.

Table 2
Details of the optical setup for the different optical techniques.

Feature	Camera	Sensor type	Filter CWL	Shutter time	Frame rate	TTL width	Px/mm ratio
‘ Schlieren imaging	Photron SA-X2	CMOS	480 nm	6.49 μs	37.5 kfps	–	4.79
OH* chemiluminescence	Andor-iStar	ICCD	310 nm	–	1 frame/inj	2.5 ms[a]	12.11
Frontal NL	Photron SA5	CMOS	390 nm	16.39 μs	37.5 kfps	–	4.80

[a]TTL-delay was set from 1.5 to 3 ms (ASOE) depending on the ignition delay.

Regardless of the applied optical technique, the general image processing is the same. However, in the pre-processing, the strategy is adapted to the particularity of each set of images.

The core of the segmentation algorithm is based on a fixed threshold intensity-sensitive method [38,39] whose principle is the image binarization with an intensity level, usually calculated as a constant percentage (or fixed threshold) of the dynamic range of a frame. The most difficult task is to achieve a proper background subtraction, especially in Schlieren, as it presents pixel structures of the same intensity level as the spray.

In the case of natural luminosity images, the background was obtained as the average of the first images before the start of injection (SOI). This is possible since the background can be considered as static during the injection event for natural luminosity images. The contour calculation is based on the independent use of two approaches that finally are combined to obtain a single binarized image where white is “spray” and black is “background”. The first approach was the only one used for natural luminosity technique and consist on the use of a fixed threshold on the intensity level of the images, and the second one is based on the standard deviation of two consecutive images in order to detect variations on the spray pixel that are stronger than the ones of the background. The images obtained were then filtered to prevent background irregularities and combined in a weighted average to obtain a final average image and the spray contour.

Fig. 6 gather different samples of the images that are obtained for Schlieren technique used to detect the vapor phase of the spray.

Flame was observed via natural luminosity from the lateral view to determine the evolution with time of the flame behavior. A sample of the images that were observed in this campaign are presented in Fig. 7, where the progression of the flame advance in the chamber is seen and the flame luminosity starts being detected near to lift-off length and then, it is extended along the spray until extinction.

The metrics has been calculated from the contours and they are different if the contour has been taken before or after the impact.

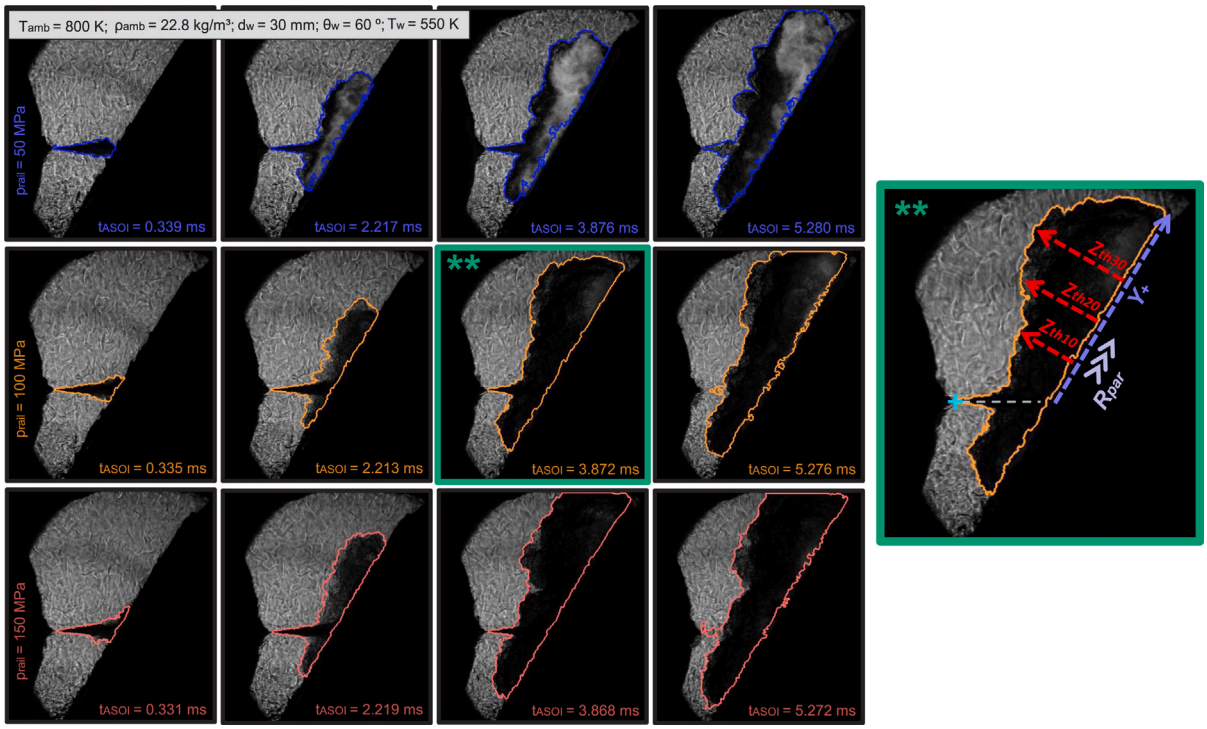

Fig. 6. Series of spray images observed via Schlieren varying injection pressure (T_{amb} = 800 K; ρ_{amb} = 22.8 kg m^{-3}; d_w = 30 mm; θ_w = 60°; T_w = 550 K). Top set: p_{rail} = 50 MPa. Center set: p_{rail} = 100 MPa. Bottom set: p_{rail} = 150 MPa. The third image at 100 MPa is zoomed in the right, in order to indicate the measured characteristics of the spray.

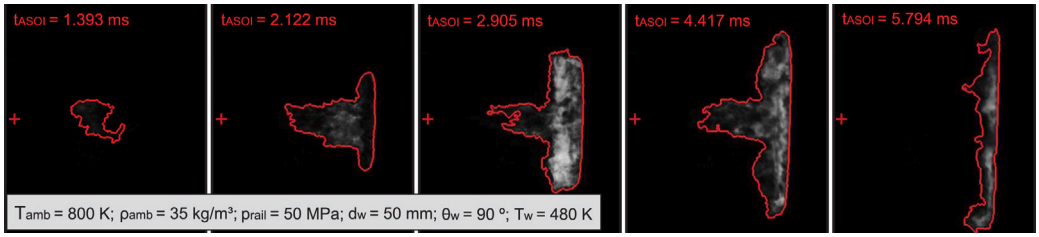

Fig. 7. Sample of the flame observed through natural luminosity (T_{amb} = 800 K; ρ_{amb} = 35 kg m^{-3}; p_{rail} = 50 MPa; d_w = 50 mm; θ_w = 90°; T_w = 480 K).

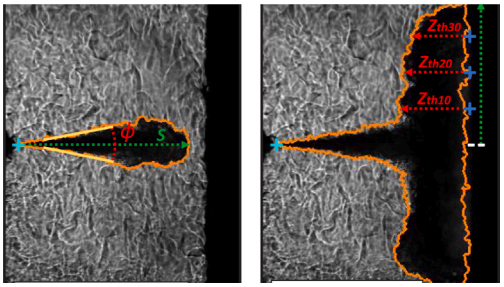

Fig. 8. Macroscopic parameters calculated from the side spray images. (T_{amb} = 800 K; ρ_{amb} = 22.8 kg m^3; p_{rail} = 150 MPa; d_w = 50 mm; θ_w = 90°; xO_2 = 0.21; Fuel = nC12). Left: Free-jet (tASOI = 430 μs). Right: Spray–wall interaction (tASOI = 2110 μs).

The variables calculated for the free-jet part of the injection event are the free-spray penetration and the spray angle and can be seen in Fig. 8-left. On the other side, the parameters that have been calculated after the start of SWI, are:

- **Spray spreading along the wall** (Y_+): The spray spreading along the wall is calculated as the distance between the 'collision point' and the furthest contour pixel in the direction towards the top of the wall respect to this point. This 'collision point' is defined as the interception between the wall plane and the free-spray axis, not being necessarily the first point of the wall that enters in contact with the spray.
- ***R-parameter* for penetration and spreading** (R_Y): In accordance with several models from spray theory [40,41], under the assumption of a cone-shaped spray, at the steady part of its evolution it can be considered that the penetration is proportional to the time rised to the power of 0.5, which makes its derivative respect to the square root of time a nearly constant value. This constant parameter to study penetration has shown to be particularly useful since it can be analyzed regardless of the considered temporal Ref. [42].
- **Spray thickness along the wall** (Z_{th}): Three consecutive points from the 'collision point' (10,20 and 30 mm) are used to measure this variable as the maximum normal distance between the wall and the spray contour.
- **Start of SWI** (τ_w): The start of the spray–wall interaction begins when the spray penetration equals the wall distance with respect to the injector tip. Nevertheless, the furthest point of the spray contour detected on-spray-axis become stagnant few millimeters before reaching the wall distance. It happens because of the strong density gradients produced in the surface of the wall by

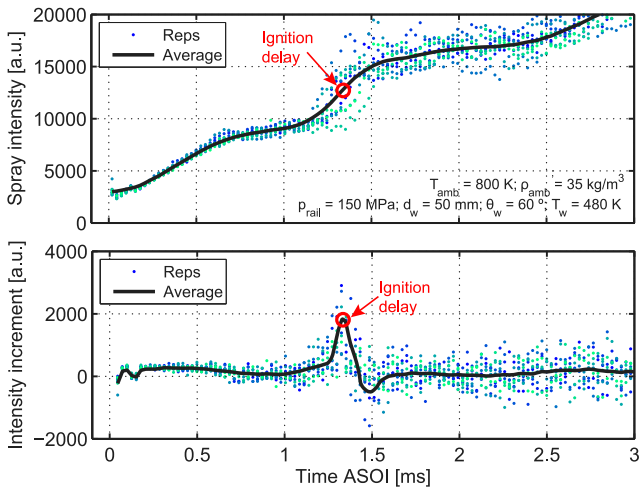

Fig. 9. Principle of calculation of ignition delay based on the evolution of the spray intensity and its derivative. Top: Spray intensity raw data per rep and averaged. Bottom: Spray intensity variation at the same conditions.

the thermal boundary layer, which limits the visualization in the nearest millimeters to the wall. To overcome it and to detect the moment when the spray reaches the wall (in on-axis terms) two approaches were used. First, from images of the wall placed in the hPhTC without heated gas flow, the real distance from the injector tip to the wall was measured (with deviations always smaller than 2 mm respect to the design dw). Then, a numerical fit was made to avoid the most transient part close to the start of the injection and the part when the spray is near to the boundary layer. This fit is then extrapolated to dw and the time when they match was taken as τ_w

- **Ignition delay (ID):** From Schlieren imaging it is possible to identify two ignition stages: the start of cool flames, when the first indications of chemical reactions occurrence take place and the second stage of ignition where high-temperature reactions occur and the spray is characterized by a rapid expansion and by the presence of high-luminosity flames. Due to that, an intensity-based image methodology has been carried out inside the detected spray contour where the pixel intensity was totalized and then derived to obtain both total spray intensity and its increment as time-resolved signals [13]. The local maximum value of the intensity increment was considered as the ignition delay reported along this work and can be seen in Fig. 9.

- **OH* chemiluminescence image processing:** The OH* images were analyzed through the approach used by Gimeno et al. [31] for Lift-off Length (LoL) calculation in free sprays. In the first place, the raw image (Fig. 10-top) is divided through the spray axis into a top and a bottom parts. Then a fixed threshold is selected. After that, a fixed radial distance in the detected spray is used for both bottom and top parts of the image to define a region of interest and the location of the leftest pixel above 50% of the max intensity in the region is taken as the lift-of length. Finally, both LoL_{top} and LoL_{bot} are averaged.

2.6. Wall temperature signal processing

Besides the image processing, the temperature signals from the two fast response thermocouples were used to obtain the surface temperature and heat flux profiles at different probe locations. The local

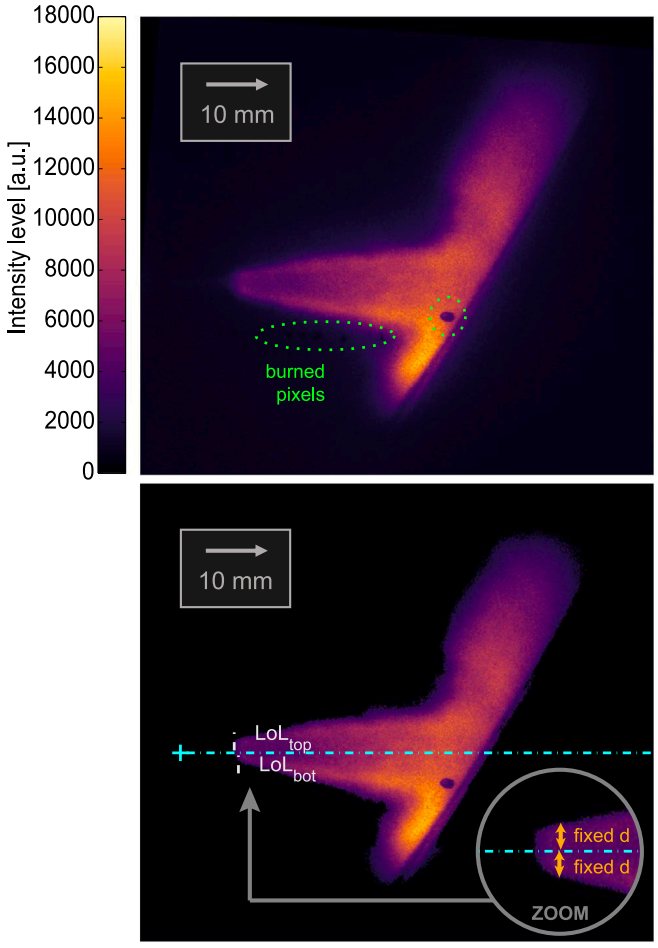

Fig. 10. OH* imaging sample and variables calculation in a set color scale (T_{amb} = 900 K; ρ_{amb} = 35 kg m^{-3}; p_{rail} = 100 MPa; d_w = 50 mm; θ_w = 60°; T_w = 550 K). Top: Raw image. Bottom: Image after being masked from binarization results.

surface temperature signals (max values around 12 mV) where directly transformed to temperature units resulting in a time and temperature resolutions of 10 μs (acquisition rate of 100 kHz), which were considered adequate for the duration of the injection and the spray–wall interaction that last approximately 3–4 ms.

The temperature data was used to compute the heat flux using MATLAB. A one-dimensional heat conduction model was considered due to:

- The flow simulation tool of SolidWorks was employed to verify the feasibility of the designed wall system, obtaining that the normal temperature gradient was much larger in comparison to the lateral one.
- The duration of the injection was too short to cause a significant radial heat flux.
- The variation of temperature in the solid wall, due to SWI takes place just in a few millimeters beyond the wall surface.

In Fig. 11 the numerical model to calculate the heat flux is shown. A finite differences method (FDM) was used to solve the parabolic partial differential temperature equation, shown in Eq. (2) to obtain the heat flux and the temperature at any wall depth and time. Where z is the coordinate perpendicular to the wall surface, T_w is the wall temperature at any point along z, and α_w is the thermal diffusivity of stainless steel,

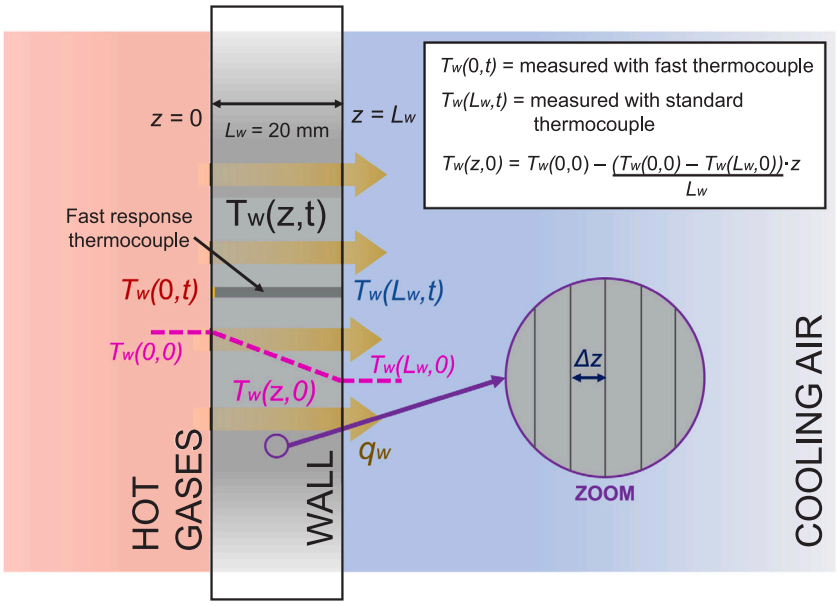

Fig. 11. Wall heat transfer model for heat flux calculation.

which is the material of the wall and matches with the reported by the thermocouples manufacturer ($3.476 \times 10^{-6}\ m^2\ s^{-1}$) .

$$\frac{\partial T_w}{\partial t} = \alpha_w \cdot \left(\cancel{\frac{\partial^2 T_w}{\partial x^2}}^{0} + \cancel{\frac{\partial^2 T_w}{\partial y^2}}^{0} + \frac{\partial^2 T_w}{\partial z^2} \right) \tag{1}$$

$$\frac{\partial T_w}{\partial t} = \alpha_w \cdot \left(\frac{\partial^2 T_w}{\partial z^2} \right) \tag{2}$$

From the known Δt of the data, the Fourier number (Fo) was kept below 0.5 as calculation stability criterion accordingly to:

$$Fo = \left(\frac{\alpha_w \cdot \Delta t}{\Delta z^2} \right) < 0.5 \tag{3}$$

Forcing Fo to 0.3, it was possible to define a spatial resolution of $\Delta z = 11$ μm, which was more than sufficient for this study. Defining $T_w(z, t)$ as function of the dimension z and the time t, the boundary conditions $T_w(0, t)$ and $T_w(L_w, t)$ were measured with the thermocouples in both the cold and hot wall faces, taking into account that the temperature of the cold face was not affected by the injection–combustion processes. From the known initial conditions $T_w(0, 0)$ and $T_w(L_w, 0)$, the initial temperature profile of the wall $T_w(z, 0)$ is estimated as the slope between those temperatures, obtaining all the needed conditions to perform the FDM.

Finally, the calculation of the heat transfer per area unit or heat flux was made from the temperature measured in the hot surface $T_w(0, t)$ and the following temperature profile in z going through the wall, as shown in Eq. (4), where k_w is the heat conduction coefficient of the wall.

$$\dot{q}_w(t) = k_w \cdot \left(\frac{T_w(0,t) - T_w(\Delta z, t)}{\Delta z} \right) \tag{4}$$

As a sample of this calculation, Fig. 12 shows a map of the wall temperature variation ΔT_w respect to the initial condition $T_w(z, 0)$, in order to show a representative case of how the solid wall temperature is disturbed by the SWI with time and how goes deep into the solid wall. As seen, and as happens in all the cases and probes, the third of the aforementioned hypothesis to ensure the 1D-model is confirmed and there was no temperature variations over 3 mm of the wall depth. Additionally, this fact justifies the use of a conventional thermocouple for the cooled face of the wall, located at 20 mm from the hot surface and helps to save computational time reducing the size of interest region.

Fig. 13 shows an example of the curves obtained using this methodology. On the top, the raw signal of the surface temperature obtained from the TC1 of the 90° wall can be seen and in the bottom the surface heat flux profile is shown.

3. Results and discussion

3.1. Ignition delay

Ignition delay vs. τ_w (both in ASOI reference) for all the points that were measured using the TRI-Wall are shown in two plots in Fig. 14. The top plot classifies the tests by ambient temperature and density and injection pressure, while right plot shows the same points differenced by wall temperatures, distances and angles. Two trends can be observed: the ignition delay is shortened by changing the ambient temperature, and on the other hand, the start of spray–wall interaction occurs before if the wall is closer to the injector. Although some other known trends, such as the increasing of τ_w and the shortening of *ID* with high densities can still be seen, the overall behaviors of the plots could

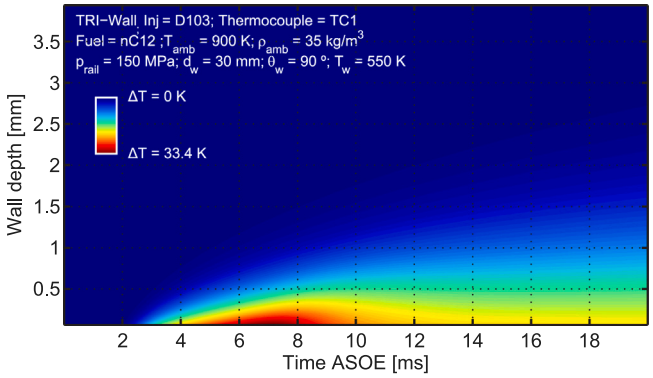

Fig. 12. Map of wall temperature variation respect to the initial condition T_w(z,0), (T_{amb} = 900 K, ρ_{amb} = 35 kg m^{-3}, p_{rail} = 150 MPa, d_w = 30 mm, θ_w = 90°, T_w = 550 K, xO_2 = 0.21, Fuel = nC12).

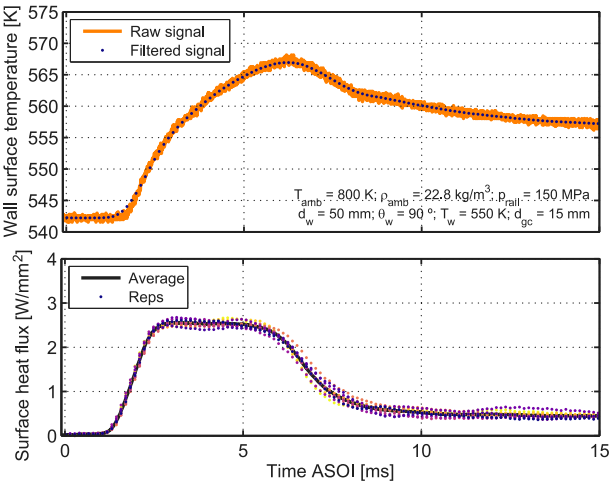

Fig. 13. Example of the heat flux and temperature variations obtained per rep and averaged. Top: Wall temperature variation respect to the initial condition $T_w(0,0)$. Bottom: Surface heat flux. The number of points of the reps has been fractioned by reducing the sampling frequency in order to avoid markers overlapping in the plot.

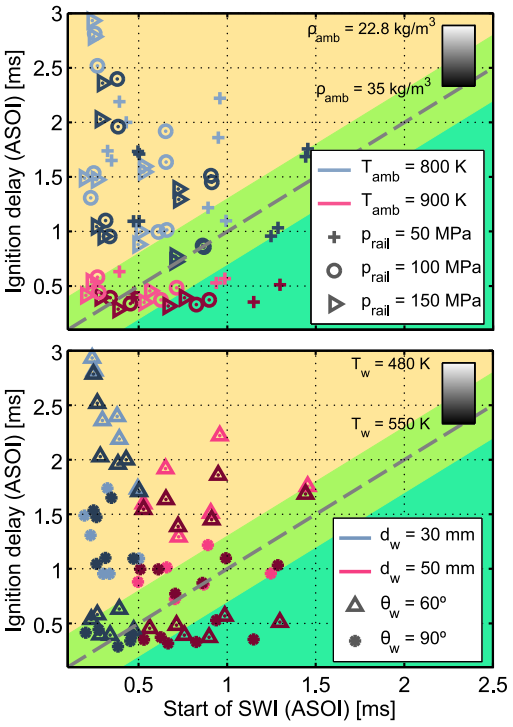

Fig. 14. Ignition delay calculated for all SWI conditions vs. τ_w and delimitation by ignition location zones (the dashed gray line represents $ID = \tau_w$). Top: Appearance based on operating conditions. Bottom: Appearance based on wall conditions.

be, in a first glance, considered not to follow clear patterns. However, the resemblance in the thermal interaction between the spray and the surroundings between both free-spray and SWI, just variating in terms of the effect of the wall on droplets break-up and spray shape evolution, made that most of the general trends remained the same. To shed light on the differences with realistic heat flux between the spray and the cooled wall, the study of ignition delay is divided into three regimes depending on the location of the spray tip when ignition occurs, as shown in the different shades of the plot backgrounds: green for sprays ignited before reaching the wall, light green for ignition given close to the spray–wall impact (between 0.3 ms before and 0.3 ms after τ_w) and yellow for ignition occurring during a well-established spray spreading onto the wall.

Fig. 15 illustrates the ignition delay at different operating conditions and for those different regimes where there was a matching spray location at the same ignition time and start of spray–wall interaction. As seen in Fig. 14, just a few points belong to the 'ignition-before-wall' regime where the spray is still in a free-spray form and the expected trends for that situation remain: ignition delay reduction with higher ambient temperature, densities and rail pressures. If ID and τ_w are similar and the points are in the 'ignition-near-to-wall' region, they seem to have the same trends of ignition delay. Actually, in the situation of 'ignition-on-wall' the trend is changed to have a longer ignition delay with higher injection pressures. This can be explained precisely by the influence of p_{rail} in determining the spray location when it ignites: while injection pressure is known to have a relatively weak effect on ignition delay, it controls the momentum-driven penetration and spreading of the spray. Therefore, once the wall is reached (which happens faster for high injection pressures), the higher the rail pressure, the greater the exposure of the spray to the cold wall. This cools down the still non-reacting spray and delays the ignition occurrence. This effect is also seen with air density which, contrarily to injection pressure, slows down the spray and diminishes spray–wall exposition, and therefore, its trend of shorten ignition delay is intensified in addition to the already known air–fuel mixing improvement. Nonetheless, ambient temperature is still the pivotal parameter on defining ignition delay behavior and the effect of other parameters barely exist at high temperature.

On the other hand, the effect of the wall configuration on ignition delay is shown in Fig. 16, similarly separated by spray tip location at ignition time. By a general observation of the three regimes, it is supported the statement of getting a longer ignition delay as a cause of a more significant exposure to the cooled wall before the ignition event. As it could be expected, in the left plot it can be seen how wall parameters have no effect on ignition delay in free-spray phase. Even when this can be apparently obvious, it is a good validation of how in-chamber conditions remain well-controlled and unaffected by the insertion of the TRI-Wall in the regions that are still far from the thermowell. From 'ignition-before-wall' to 'ignition-on-wall', the strength of parametrical variation effects on ID gradually increases: once SWI is well-established, shorter wall distances imply that the spray enters before in contact with the cold wall, which delays the posterior ignition. Wall temperature effects seem to be negligible. Although a weak trend leads to think that the lower T_w is, the longer the ignition delay, and this behavior could be interpreted as a stronger spray cooling; those differences are too weak to be considered out from the experimental deviation fringe. The author considers that the difference between the two wall temperature conditions of the test matrix (70 K) is still too low to have significant ignition delay gaps. This is in accordance with Chen et al. [43], where authors observed slight variations on ignition delay with wall temperatures differing as much as 250 K, and at considerably low ambient densities (18.03 kg m^{-3}), if compared to the test plan of this work.

A non-obvious but very clear trend is that ignition delay is longer for a wall angle of 60° than for 90°. To illustrate a possible explanation of this, Fig. 17 shows different Schlieren image backgrounds of two wall configurations (two wall angles at 50mm wall distance) for 800 K (top) and 900 K (bottom images). To get these images, the background has been averaged by taking all the frames before SOI of all repetitions independently of rail pressure. This average image allows to largely suppress dark structures caused by the in-chamber density inhomogeneities, characteristic of Schlieren imaging. Green dotted lines in the figure represent the wall edge observed with the hPhTC with no hot flow (valves closed, heaters turned off), which was the original condition in which the wall was set and where the geometrical features of the image were determined for processing (injector tip and wall location, processing masks, etc.).

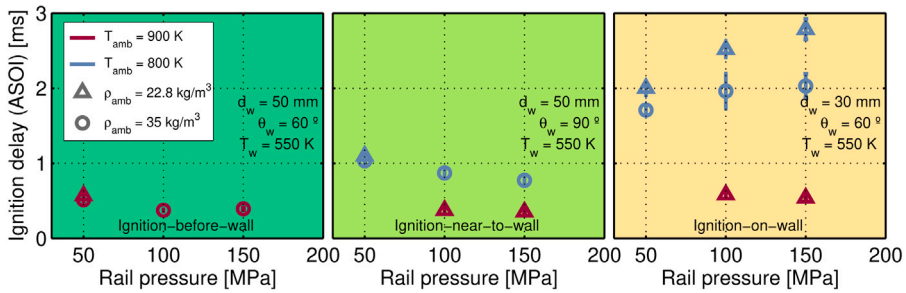

Fig. 15. Ignition delay vs. injection pressure for different air thermodynamic conditions and ignition location zones. Left: Tests with ignition before reaching the wall. Center: Tests where ignition takes place close to the wall. Right: Ignition occurs in well defined SWI.

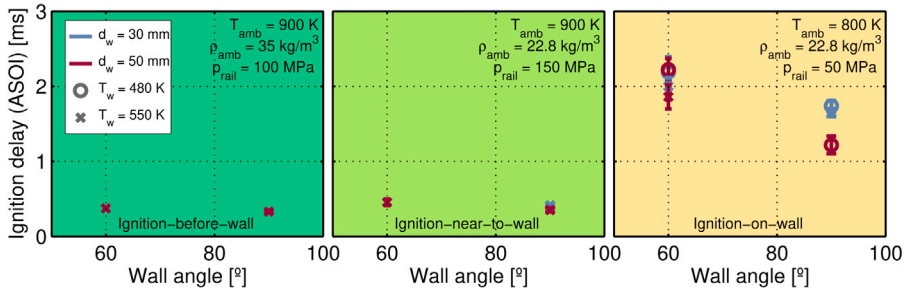

Fig. 16. Ignition delay vs. wall angle for different air wall distances, temperatures and ignition location zones. Left: Tests with ignition before reaching the wall. Center: Tests where ignition takes place close to the wall. Right: Ignition occurs in well defined SWI.

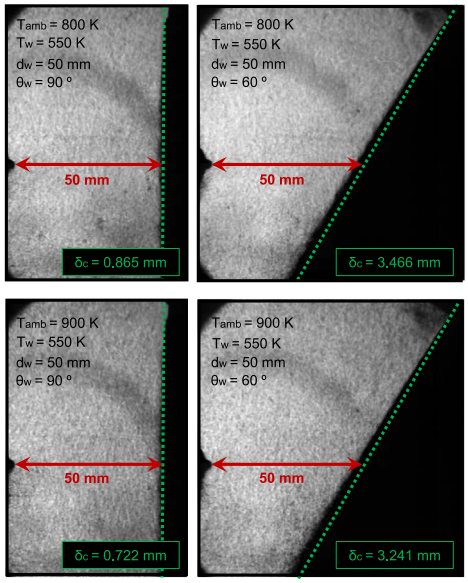

Fig. 17. Averaged Schlieren imaging background at $\rho_{amb} = 22.8\,\mathrm{kg\,m^{-3}}$ and various gas temperature and wall conditions. Top: $T_{amb} = 800\,\mathrm{K}$. Bottom: $T_{amb} = 900\,\mathrm{K}$. The green dotted lines represent the original wall edge taken with no hot gaseous flow into the vessel.

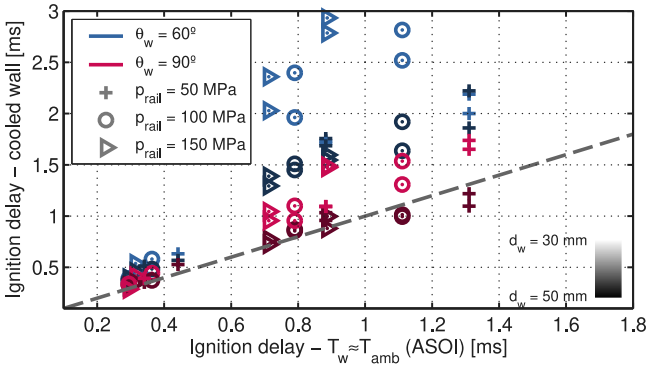

Fig. 18. Ignition delay calculated for all tests with the TRI-Wall.

In the images, a dark layer is seen onto the wall respect to the original position, due to Schlieren light deviation. This layer evidences a strong density (i.e. temperature) gradient in the vicinity of the wall. Similarly as done with the spray, the contour of this layer was obtained, which allowed to obtain a value of the average boundary layer thickness δ_c respect to the original wall surface (0.85 mm in the case of 90° and 3.63 mm in the case of 60°). This boundary layer is very thin in the perpendicular wall cases as can be seen in Fig. 17. The layer for the inclined wall seems to be thicker in the bottom and narrower in the top of the wall, as well as it is significantly thicker than in the perpendicular wall case. As it is known, hot air is less dense than cold air, which makes that in an ambient with temperature gradients, heavier cold air molecules tend to go towards the wall bottom due to gravity and hot air ones to be pushed upwards. This effect is not visible in the free-zone background due to the in-chamber temperature homogeneity of the vessel and the larger and stochastic effect of the flow over the temperature one. Nevertheless, onto the inclined cold wall, the surrounding air is cooled down and instead of just going downwards, the slope of the wall and the air stagnation on it accumulate those cold air particles onto the wall, in a larger extent on the wall bottom due to their weight. This layer of cold air represents through convection a significant contribution to the heat transfer from the air–fuel mixture, delaying it to reach ignition conditions.

Fig. 18 compares the ignition delay obtained by the use of the two different wall hardware: the wall presented in this work and a wall made of quartz presented in a previous work [44]. The quartz wall allowed to have nearly isothermal conditions during the injection event and a wall temperature similar to the ambient one, so this work is used hereinafter as a reference for this experience that isolates the phenomenon from the spray/wall thermal interaction, as it has been

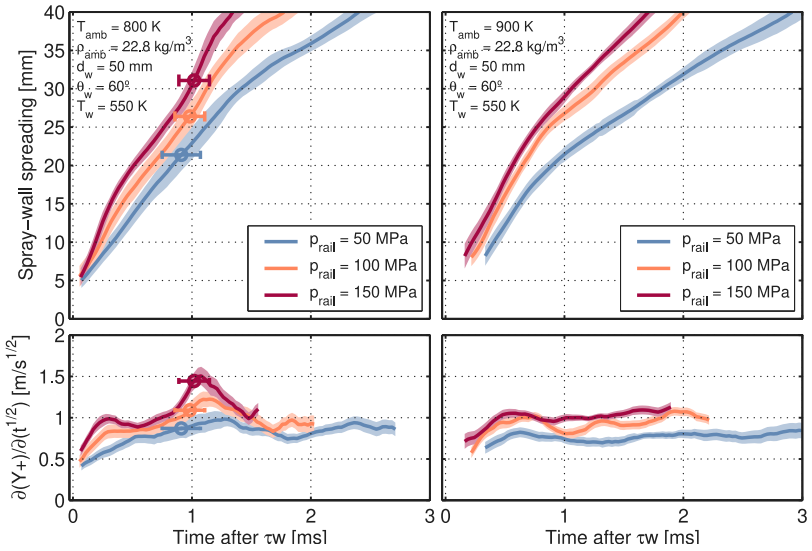

Fig. 19. Reacting spray spreading (top) and its respective *R-parameter* (bottom) for different injection pressures and ambient temperatures (ρ_{amb} = 22.8 kg m^{-3}; d_w = 50 mm; θ_w = 60°; T_w = 550 K). Left: Air temperature at 800 K. Right: Vessel set at T_{amb} = 900 K.

made with a similar test matrix and employing the same facility and injector. Short ignition delays are still similar in both cases. The effect of collision-induced break-up is the same for both walls, which makes the larger difference of the wall distance effect to be produced by the earlier exposure to the cold wall, which delays ignition. This spray–wall contact that causes longer ignition delays is intensified by high injection pressures, in opposition to its known effect that accelerates ignition start. In terms of wall parameters, the strongest parameter that affects *ID* is the wall angle due to the enhance on spray cooling caused by the cold air layer formation in the inclined wall. In comparison to a diesel engine, this nearly quiescent vessel with a static wall may develop a more significant layer. Nevertheless, in automotive engine architectures, it is quite common for spray orientation to be downwards and the bowl geometry could lead to colder air regions.

3.2. Spray evolution on the wall

In Fig. 19, spray spreading onto the wall is observed for points at different injection pressures and at T_{amb} = 800 K (left) and 900 K (right), along with their respective *R-parameters*. For all the figures similar to Fig. 19 presented in this work, the circle symbol represents the point where the ignition delay occurs. Also, the shaded area, present in all the figures, represent the standard deviation for each performed condition. The higher the injection pressure, the higher the spray velocity at the nozzle outlet and the spray momentum flux during both free-spray phase and SWI [45]. Differences with ambient temperature are given by ignition delay in terms of when those variations on spreading happen, and how intense and prolonged they are (more air-fuel premixing time drives to a more vigorous expansion [46]). It is important to take into account that, in addition to the spray momentum, the crossed effect of injection pressure on ignition delay (spray flow enhanced turbulence against larger spray area in contact with the cold wall) affects spreading. The acceleration phases that characterize reacting diesel spray advancement are still seen: A first phase after the start and stabilization of the injection in which the R-parameter presents a pseudo-constant pattern, shortly starts an evident rise in which the ignition delay occurs, then the spray decelerate and increases its advancement until a quasi-stable R-phase. Last, this R value is greater than the stable one reached in the first before-reaction phase, which indicates that besides the acceleration obtained in the bump, the spray in the stable zone of combustion is also faster than in its first steady phase [47].

On the other hand, Fig. 20 illustrates wall spreading when both ambient density and wall temperature are changed. First, density promotes gas entrainment into the spray, making its spreading slower, while it shortens *ID* by both representing a higher ambient pressure (at the same gas temperature and oxygen fraction) and by reducing spray exposure to the low temperature wall. This delay on ignition at low ambient densities increments the premixed combustion phase and contributes to the spreading boost respect to the high density environment. Wall temperatures of 480 K and 550 K do not exhibit either significant differences on ignition delay as previously stated, an consequently nor differences on spray spreading. First, having similar ignition delays, there are not variations produced by different pre-mixing levels. Additionally, the thickest mean boundary layers measured are around δ_c = 3.63 mm (being significantly less for perpendicular cases and linearly decreased as go further along the wall). Taking into account that spray thicknesses are in the order of $Z_{th10} \approx$ 15 mm and increase at further measuring distances, it can be understood how the density gradient of the thin layer has no important effects on spray advancement onto the wall [48].

Different wall distances and inclinations, and their effect on spray spreading is shown in Fig. 21. Points with short ignition delays are shown in an attempt to reduce the effect of ignition timing. Sprays on the 60° wall are faster in the measured spreading direction, as it is expected. As discussed, the effect of the boundary layer increment with wall inclination (where gases density is locally higher) on spray spreading is negligible. At the same time, the only effect on spreading of wall distance that can be seen in the plots, is given by ignition delay in terms of the changes on τ_w, which is the time reference employed for the horizontal axis, and the crossed effects of a shorter wall distance: a sooner spray opening which provokes a wider exposure to hot and dense air, versus the sooner and longer contact of the spray and the cold wall.

Figs. 22; 23 and 24 depict the behavior of the vapor thickness of the spray onto the wall at reacting conditions with wall cooling. Fig. 22 shows in the left the effect of gas temperature and in the right the influence of injection pressure variations. Ambient temperature do not have effect until ignition, when the spray have a general expansion and an increment in its growth rate. As seen, this happens before in the high temperature case but the 800 K point has a longer premixing time. This effect is also seen with injection pressure, which has the aforementioned effects on ignition delay depending on its spreading on the wall and no more representative influences on spray thickness. In

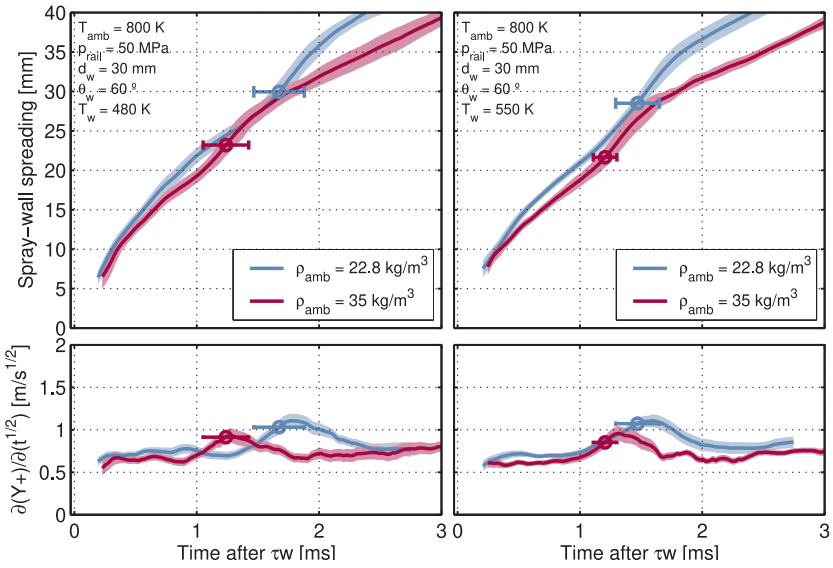

Fig. 20. Reactive free penetrations (top) and their *R-parameter* (bottom) for various fuels and air densities (T_{amb} = 800 K; p_{rail} = 50 mm; d_w = 30 mm; θ_w = 60°). Left: Tests at T_w = 480 K. Right: Wall set at 550 K.

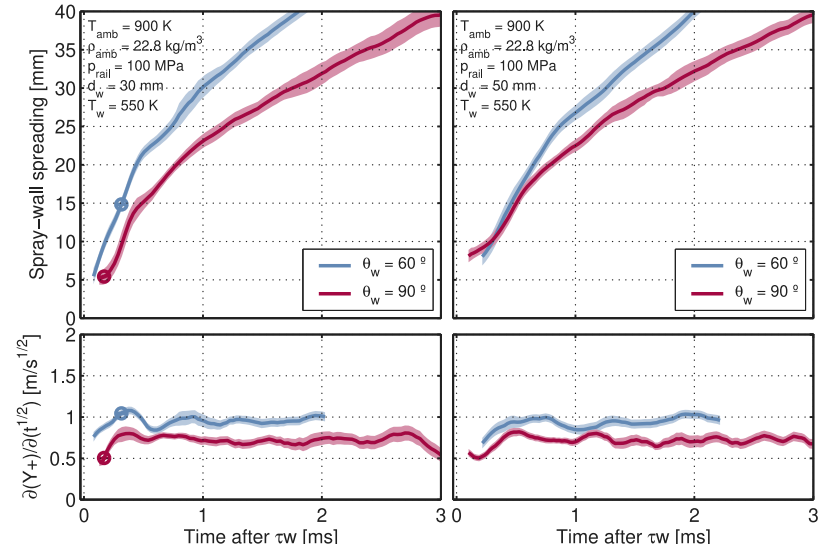

Fig. 21. Reactive spreading (top) and their *R-parameter* (bottom) for different wall positions (T_{amb} = 900 K; ρ_{amb} = 22.8 kg m^{-3}; p_{rail} = 100 MPa; T_w = 550 K). Left: Tests with injector-wall distance of 30 mm. Right: Points with the wall located at 50 mm from the injector tip.

the shown case, the most different point in regards to spreading velocity and *ID* (timing and premixing time) is the set at 50 MPa injection pressure, which is directly related to the shown spray thickness. Ignition delay is again the pivotal parameter to define how combustion-driven expansion is provoked, which therefore makes the ambient temperature effect the strongest of all [13,15].

The effect of varying both gas density and wall temperature is reflected in Fig. 23. When gas density is raised, atomization is improved and the spray spreading on the cold wall gets slower, all facts that promote shortening on ignition delay, after that event takes place, still a more intense gas entrainment is given at higher gas density, with a noticeable impact on spray thickness. On the other side, wall temperature does not have a substantial effect on spray thickness as it could be expected since it does not affect ignition delay or spreading, and also by taking into consideration that the effect of gas temperature is only given by the changes on *ID* and not by other mechanisms of SWI.

Different wall positions are illustrated in Fig. 24, by changing the injector-wall distance (left) and the wall inclination angle (right). In the set of the left, it can be seen how the case is very similar as the observed for gas temperature: there is no substantial effect in the very beginning of the inert phase of thickness. Nevertheless, the ignition delay in the plot is longer for the 30 mm case, due to both the gap in the temporal references of the curves and the sooner spray cooling. However, thickness is similarly affected by wall distance in regards to both cases having stages with different air entrainment rates. Additionally, in SWIs at non-reacting conditions, the main effect of impingement angle on thickness is given by the transitoriness of the spray–wall interaction due to the deviation of the spray advancement direction. In those cases, this is not well-differenced for various angles since *ID* was unaffected by them. In the present case, the perpendicular wall has the most abrupt change of direction in the spray momentum but, on the other side, ignition gives place to a new transitoriness that is delayed and more intense for the inclined wall with a longer premixing phase.

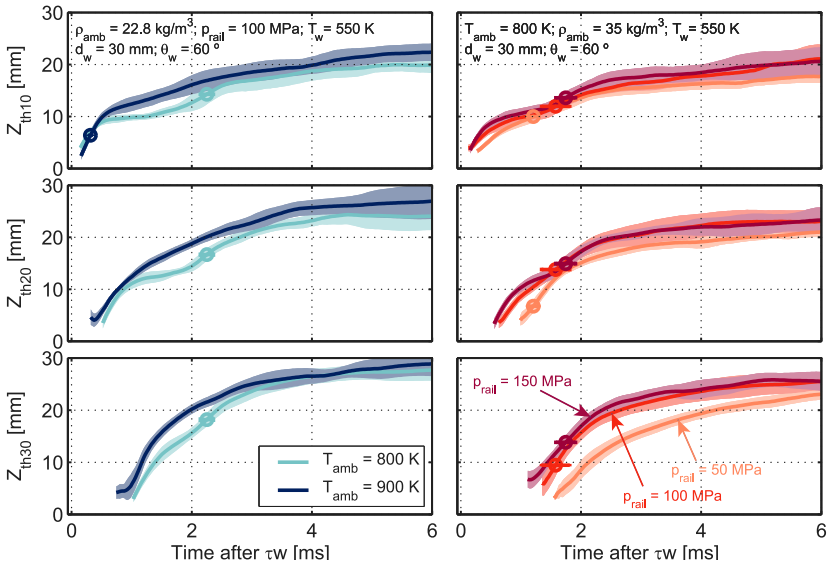

Fig. 22. Spray thickness for different ambient temperatures and injection pressures (d_w = 30 mm; θ_w = 60°; T_w = 550 K). Left: Temperature variation at ρ_{amb} = 22.8 kg m^{-3} and 100 MPa. Right: Different injection pressures at ρ_{amb} = 35 kg m^{-3} and 800 K.

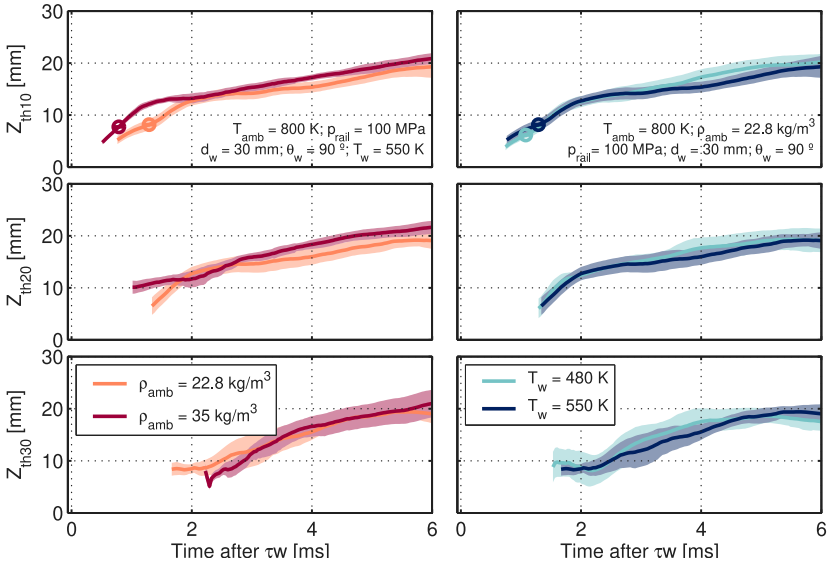

Fig. 23. Spray thickness for different gas densities and wall temperatures. (T_{amb} = 800 K; p_{rail} = 100 MPa; d_w = 30 mm; θ_w = 90°). Left: Different gas densities at T_w = 550 K. Right: ρ_{amb} = 22.8 kg m^{-3} at two different wall temperatures.

3.3. Flame morphology visualization

As explained in the first sections of this work, the camera used to record the natural luminosity has been configured with a long shutter time in order to detect flame regions with low intensity and precursor chemical reactions at the beginning of the exothermic processes that lead to combustion.

Flame was observed to determine the evolution with time of the flame behavior. A sample of the images that were observed in this campaign are presented in Fig. 7 and in Fig. 25, where the progression of the flame advance in the chamber is seen and the flame luminosity starts being detected near to lift-off length and then, it is extended along the spray until extinction. In Fig. 25 is possible to observe the effect of flame propagation over the inclined wall and the formation of the vortex at the end of the flame front.

A first analysis was made by observing the effect of ambient temperature and injection pressure on the thickness of the sooty flame in Fig. 26. As it has been done throughout the manuscript, the shown thickness is measured at 10 mm; 20 mm and 30 mm from the 'collision point'. Fig. 26 continues showing a thicker flame for high ambient temperature cases, as expected from the enhanced ignition respect to the T_{amb} = 800 K point, as well as the longer flame life of the first one due to its sooner start of combustion. In this case at θ_w = 60°, the ignition is so delayed due to the cold air layer formed, that the vortex in the curves of the low temperature point can barely be seen. Nevertheless, the profile is still the same: the tip vortex represented with a peak and then, a semi-stable thickness. Injection pressure, on the other side, still reduces the vortex duration and the general soot thickness observed via natural luminosity accordingly to [49]. This effect is seen to be intensified as the flame is exposed at higher pressure and velocity to a cold wall, which reduces the overall mixture temperature at the wall vicinities.

Fig. 27 reflects how flame thickness is affected by a change of ambient density and wall temperature. In Fig. 27-left it is seen how

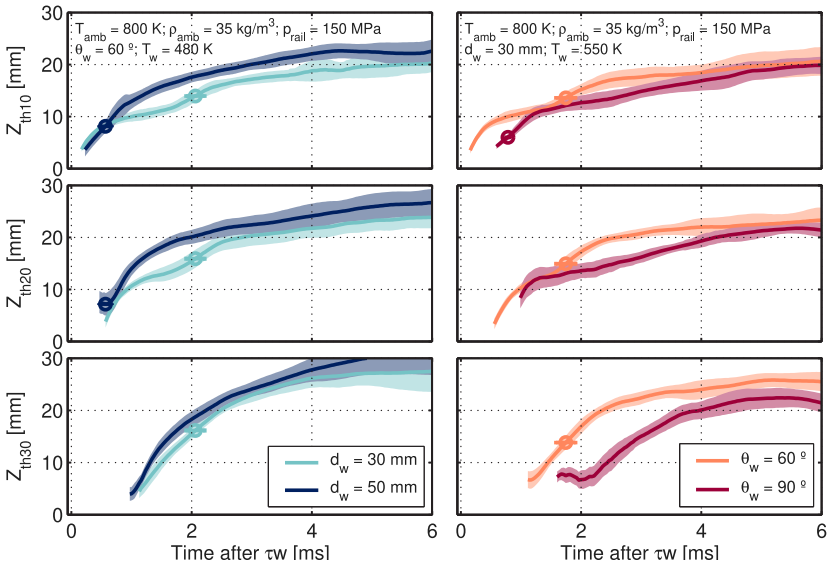

Fig. 24. Spray thickness for different wall positions. (T_{amb} = 800 K; ρ_{amb} = 35 kg m^{-3}; p_{rail} = 150 MPa). Left: Different wall distances from the injector tip for θ_w = 90° and T_w = 480 K. Right: Different wall angles fixing d_w = 50 mm and at T_w = 550 K.

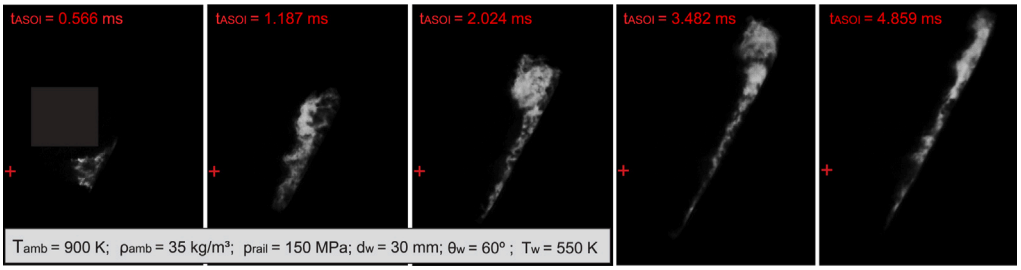

Fig. 25. Sample of the flame observed through natural luminosity (T_{amb} = 900 K; ρ_{amb} = 35 kg m^{-3}; p_{rail} = 150 MPa; d_w = 30 mm; θ_w = 60°; T_w = 550 K).

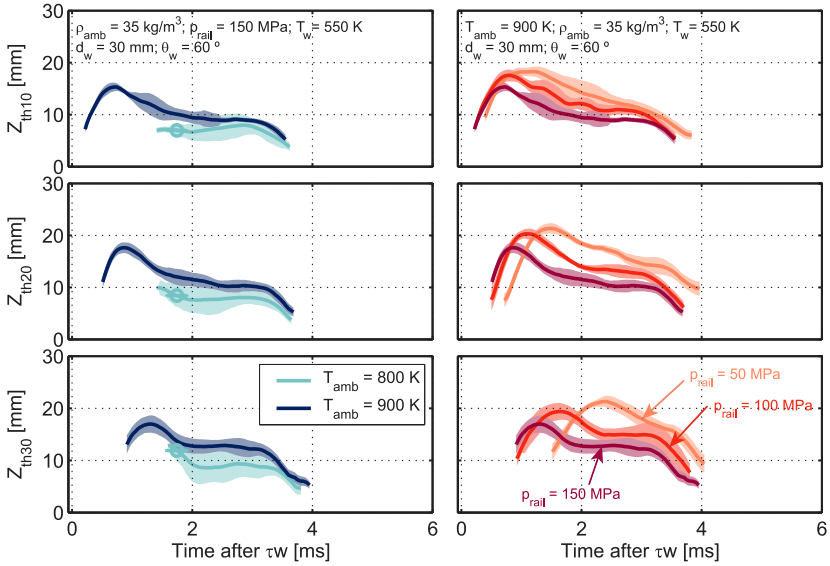

Fig. 26. Flame thickness at various ambient temperatures and injection pressures (ρ_{amb} = 22.8 kg m^{-3}; d_w = 30 mm; θ_w = 60°; T_w = 550 K). Left: Temperature changed at 150 MPa. Right: Different rail pressures at 900 K.

as the spray moves farther onto the wall, not only flame thickness is slightly growing in general, but the frontal vortex is getting a more defined shape in its way along with the fact of thickness being narrower at lower air densities due to the relative lower gas entrainment rate. This Z_{th} is, in all measuring points, decreasing when wall temperature drops. Even while several previous parameters do not seem to be notably affected by wall temperature in the range of control, the flame is narrow enough and in direct contact with the wall to be appreciably

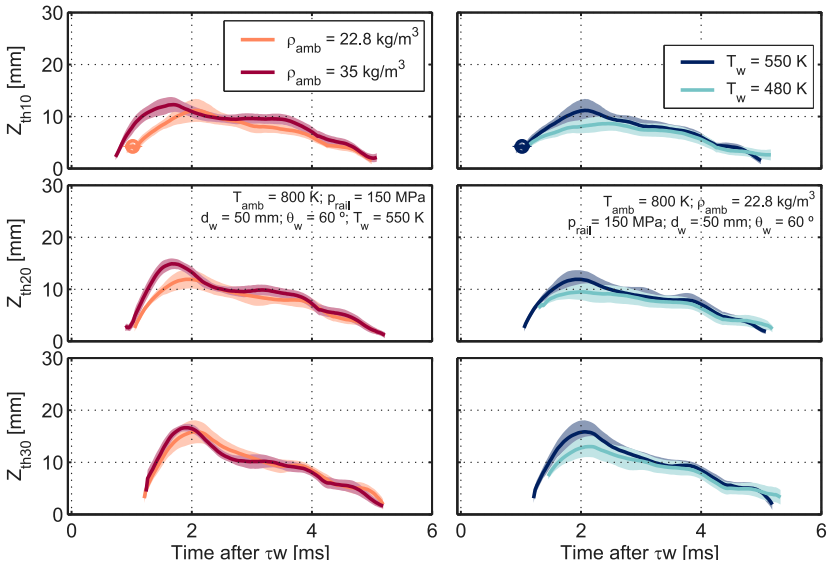

Fig. 27. Flame thickness for various gas densities and wall temperatures. (p_{rail} = 150 MPa; d_w = 50 mm; θ_w = 60°). Left: Different gas densities at T_w = 550 K. Right: ρ_{amb} = 22.8 kg m^{-3} at two different wall temperatures.

affected within the test plan targets (with around a 15% of thickness reduction).

Different wall distances and angles were set in the test points shown in Fig. 28. At a constant wall angle and temperature, the effect of placing the plate further from the injector tip makes the flame thicker. Nevertheless, in regards to wall angle, the differences between points of different wall inclinations is not obvious. In counter-position to the inclination which promotes a thicker flame formation due to its lesser transitoriness and higher spreading velocity, the notably thicker boundary layer, defined as the cold air zone that remains accumulated on the wall, has a similar effect than the aforementioned for wall temperature. In this case, the boundary layer effects are stronger in the inclined wall, respect to the perpendicular wall, where its thickness is about 3 times narrower. It has to be considered that boundary layers of 60° wall cases are commonly as thick as the 34% of the steady (upstream from the front vortex) flame thickness onto the wall. Additionally, in perpendicular wall cases, due to the lateral view, the steady thickness after vortex is more covered by the front that is produced by the lateral spreading of the flame.

3.4. Lift-off length

The overall behavior of lift-off length in this campaign is shown in Fig. 29, where the left set depicts variations on operating conditions such as ambient density, temperature and rail pressure for two different wall settings (top and bottom), while the right set illustrates parametrical variations related to wall characteristics such as its inclination angle in the horizontal axis, wall distance from the injector tip and wall temperature. The strong influence of the thermodynamic conditions of the surrounding air is maintained, shortening *LoL* with density and mainly with temperature increases.

Negligible influence on *LoL* from the side of wall temperature in the TRI-Wall cases is also observed, which agrees with the behavior of ignition delay previously shown [22] due to the reduced difference between the target points. This null effect of the wall distance or impingement angle on points with short ignition delay, as a lack of the re-entrainment of the burned products in a flat wall has been reported in other works [50,51]. Again, it has to be taken into account that the shown points are only the ones with visible lift-off length that are short enough to not being covered by the very thickness of the spray part which is in interaction with the wall. Unfortunately, the architecture of the TRI-Wall makes the frontal view of the spray not optically accessible, which do not allow to obtain quantitative data about lift-off lengths close to the wall or that surpass wall location in free-spray situations.

In the study of Peraza et al. [44] the fundamental physical–chemical mechanisms that define lift-off length location were analyzed using a setup in which $T_{amb} = T_w$, obtaining similar results as the one described in this work. Fig. 30 is helpful to compare both situations in regards to visible *LoL*. Short lift-off lengths are not affected by the wall, which is logic taking into account that they are far from it and the reacting zone is not affected by its considerably lower temperature, considering that the wall has demonstrated to not be intrusive with the ambient temperature homogeneity into the chamber. Nevertheless, as lift-off length becomes larger, it is noticeable how the values obtained by employing the TRI-Wall increase which indicates that temperature of the air-fuel mixture for the wall at 50 mm starts to be affected by the cooled wall at around 22 mm from the wall and increasingly more as the *LoL* gets closer. Under this perspective, injection pressure is secondarily prone to enlarge lift-off length due to its trend to push this zone nearer to the cooled wall, while the exact opposite happens with gas density. In Fig. 30, this lift-off length difference between the two hardware is confirmed to be produced by spray cooling observing that, similarly as happens for ignition delay, short *LoLs* are not affected by wall angle while the closest to the wall are slightly larger for the inclined wall, presumably due to the effect of the thicker cold air layer that is formed onto the wall. Moreover, this was an evidence of the greater heat transfer potential of the two-phase air–fuel mixture respect to the air into the chamber, whose temperature demonstrated to remain homogeneous and unaffected by the colder wall temperature except for the region approximately at 3 mm from the wall.

3.5. Flame-wall heat flux

The time resolved wall temperature was registered with the two fast-response thermocouples TC1 and TC2 at two locations per wall. Those locations were different depending on the wall employed, accordingly to the scheme shown in Fig. 4. The temperature signal was directly used to compute the heat flux transferred to the wall by the flame. Both wall temperature variation ΔT_w respect to the initial one (setted accordingly to the test plan and measured by the thermocouples before SWI) and the wall heat flux $\dot{q}_w$ are shown in the following plots for different parametrical variations. In all the following images, the

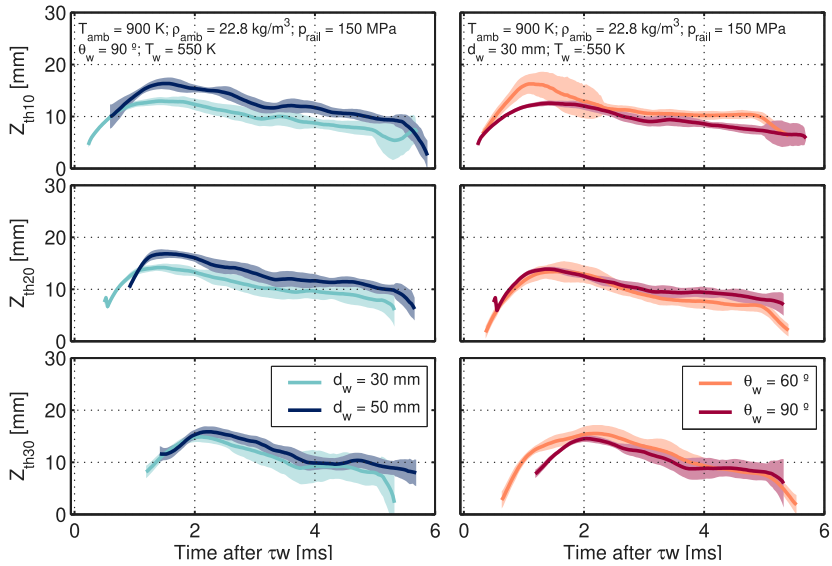

Fig. 28. Flame thickness for different wall positions. (T_{amb} = 900 K; ρ_{amb} = 22.8 kg m^{-3}; p_{rail} = 150 MPa). Left: Different wall distances from the injector tip for θ_w = 90°. Right: Different wall angles fixing d_w = 30 mm.

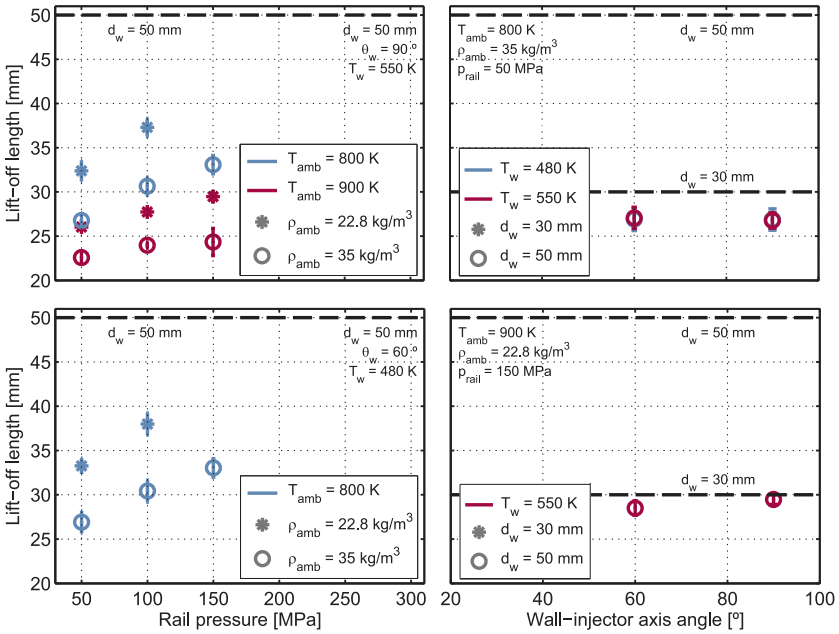

Fig. 29. Lift-off length obtained for different parametric changes. Left set: *LoL* vs. injection pressure at different gas temperatures and densities. Right set: Variation of *LoL* vs. wall angle at different wall orientations and temperatures. Please note that wall locations are shown in dashed black lines.

top pair of plots corresponds to the measures made by TC1 and the bottom set comes from TC2.

On the first place, the effect of setting different ambient temperatures is shown in Fig. 31. As seen, the general profile of the wall temperature variation from the test target was a slope rise when the spray flame enters in contact with the sensor. This slope gradually decreases to finally reach a peak. After this maximum ΔT_w, wall temperature starts to slowly decrease as a result of flame extinction in that injection event [29,52]. Although the plot only shows the first 15 ms after the start of spray–wall interaction, it has been verified that the time set between injections (4000 ms) is more than enough to reestablish the wall temperature to its target value. In the right set of Fig. 31 the profile of the heat flux is observed, where a strong rise is followed by a nearly constant value during the quasi-steady phase of the flame-wall heat transfer, profile that is in agreement with the findings of [53–55]. Once the flame is extinguished, heat flux dramatically drops to a low level where heat flux is driven by the gases that remains near the wall in movement, resulting into a higher convective coefficient than the values before SWI. Finally, it can be seen how for the sample that is shown in the figure, the heat flux is higher as the probe is located closer to the geometrical center of the wall defined as 'collision point'. This distance is shown in the upper part of each graph as d_{gc}. The two sensors are reached at post-impact velocities that, as previously discussed, are considerably lower than pre-impingement velocity, and it decreases as the spray advances further from the impingement location.

In regards to the effect of ambient temperature on ΔT_w and $\dot{q}_w$, the higher T_{amb} is, the fuel has in proportion a longer diffusion flame. Higher ambient temperatures lead to higher reactivity and also higher flame temperatures. This represents not only a more significant temperature variation but a stronger heat flux to the wall. Nevertheless,

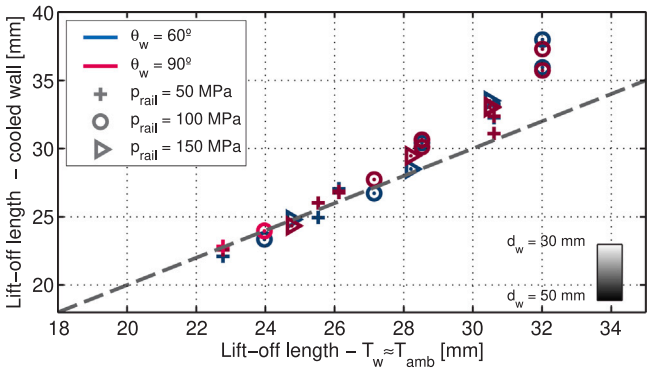

Fig. 30. Lift-off length measured for the visible tests with the TRI-Wall.

the duration from the start of the quasi-steady heat flux to the flame extinction is quite similar for both gas temperatures.

Another difference can be seen when gas density was changed, as illustrated in Fig. 32. Ambient density promotes an enhancement on fuel atomization. It induces not only a higher reactivity but also a stronger gas mass flow in entrainment into the flame during the combustion that boosts the energy release to the wall. Wall exposure to a higher air mass flow is also a factor to be taken into account. Furthermore, density affects the Reynolds number, which directly influences the convection coefficient of the hot gases.

Fig. 33 shows the effect of increasing p_{rail}. Turbulence promotes a sooner ignition and the effect on ΔT_w is in a first order, produced by the faster flame spreading onto the wall surface, which affects the convection heat transfer coefficient and finally, increases the wall temperature rise at higher pressures. The same occurs for the measured heat flux, that has a steeper slope and a higher stable value at elevated injection pressures. This quasi-steady phase part of the signal is longer at high injection pressures, due to the relative time when that phase is recorded by the sensor (sooner for high pressure–velocity sprays) and the nearly similar flame extinction.

On the other side, in Fig. 34 it is shown how the wall temperature has a negligible effect on the heat flux, which happens for all points. This, it is in accordance with previous behavior seen in different combustion parameters that would be driven in a large extent by the heat transfer with the wall (such as ignition delay, spray expansion, etc.), except by flame thickness. This can obey different facts: first, as stated before, the difference between the two target wall temperatures T_w is too low to cause a significant variation. It has to be taken into account that, in the case of target gas temperature difference (900 K - 800 K), it is not just larger but it produces a huge increment on flame temperatures [56–58], which is in contact with the wall. The difference on those wall temperatures by rising T_{amb} in 100 K is just around 3-5% depending on the point and the thermocouple location. Wall temperature is not the only reduced, but the flame is cooled down too, which supports that δT between the flame and the wall is not significantly different for both wall temperatures and, assuming a similar spray velocity from the spreading results, it is expectable to observe similar heat flux by changing the target wall temperature.

Fig. 35 shows the variations in surface temperature and heat flux when the wall is at different distances from the injector tip. For a larger d_w, the temperature and heat flux variation seem to be increased for the points shown in the figure and consistently for the whole test matrix. This effect could be out of the expected behavior, taking into account that, as at $d_w = 50$ mm the thermocouple is further away from the nozzle, turbulence (i.e. convection coefficient) could be foreseen to be lower. However, from Schlieren results it was observed how since the beginning of SWI, and therefore since the spray tip is located at the 'collision point' or $d_{gc} = 0$ mm, the spray tip spreading is approximately the same regardless of d_w and then, the convection coefficient may not be largely affected by a significant variation of velocities for sensors located at the same d_{gc} and wall inclination. On the other hand, a possible explanation of the observed behavior of heat flux can come from the temperature distribution inside the flame. It has been observed how the wall distance had a negligible effect on visible lift-off length and then, thermocouples are located further downstream from it in the $d_w = 50$ mm case respect to the 30 mm. The inner gases inside the diffusion flame could be expected to be hotter in locations further from the *LoL* region [18,59] and that is something that is also given in the combustion structure of an impinging flame [60,61]. This factor, together with the low variation on spray velocities at each thermocouple location for different wall distances, could be considered a suitable explanation for the observed trend.

Finally, Fig. 36 shows both surface temperature rise and the heat flux for walls with different inclination angles. It has to be considered that the two fast thermocouples are differently located depending on the wall, as labeled on the top of each graph. That is the first difference between the signals of different wall angles to be taken into account, as it is known that ΔT_w and $\dot{q}_w$ drop in the radial spreading of the spray due to the higher level of spray-sensor contact and the gradual velocity losses. Nevertheless, wall inclination induces a non-homogeneous momentum distribution that favors the upper part of the spray. For the inclined wall, TC1 (top plots) is placed at 15 mm further than for the inclined wall at 90°, but that is compensated in terms of tip velocity by the wall inclination of the first one. Something similar happens for TC2 (bottom graphs) which is similarly distanced from the geometrical center for the two walls ($d_{gc} = 18$ mm and $d_{gc} = 20$ mm respectively), what would make the spray velocity higher at the sensor location for the inclined wall. Even when, in the 60° wall, TC2 location is on the side and not aligned in the measured spreading axis, the inclination of spreading in the direction from the center to the thermocouple is still between 60° and 90° (actually 73.4°). These observations on the spreading velocity for each thermocouple are in accordance with the temperature rise observed in Fig. 36.

In regards to the wall heat flux, the thermal boundary layer strongly delays the ignition and, because of that, the duration is shorter for the inclined wall. Nonetheless, this layer can be considered to be displaced from the wall by the high-momentum spray. In the 60° case it is even observed how the spray reaches the sensor pushing hot air at high velocity near to it and then, when the ignition takes place, the slope of the heat flux is dramatically increased. As expected, the inclined wall reaches a higher heat flux due to the spray velocities described above in terms of tip spreading.

4. Conclusions

A thermo-controlled and instrumented wall with two fast-response thermocouples has been used to characterize the behavior of the spray–wall interaction at engine-like operating conditions.The test matrix was selected taking into account several points of interest for the ECN community for diesel applications. The wall design used in the experimental campaign allowed to test two different wall angles, two distances between the 'collision point' and the injector tip, and two different wall temperatures by regulating the coolant flow in the cold-external face of the wall system. Performing simultaneously flame visualization via natural luminosity, spray visualization recording Schlieren images, lift-off length by the detection of the OH* radicals employing an intensified camera and a 310 nm narrow filter and, finally, a time-resolved heat flux calculation from the signals of the temperature sensors located at different points of the wall. Regarding the results obtained through this work:

- The exposure to the cold wall affects the ignition delay according to the following parameters: high injection pressures make the spray spread further onto the wall increasing the spray–wall contact causing a cooling of the spray delaying the ignition. Contrarily to the injection pressure, the increases in the air density

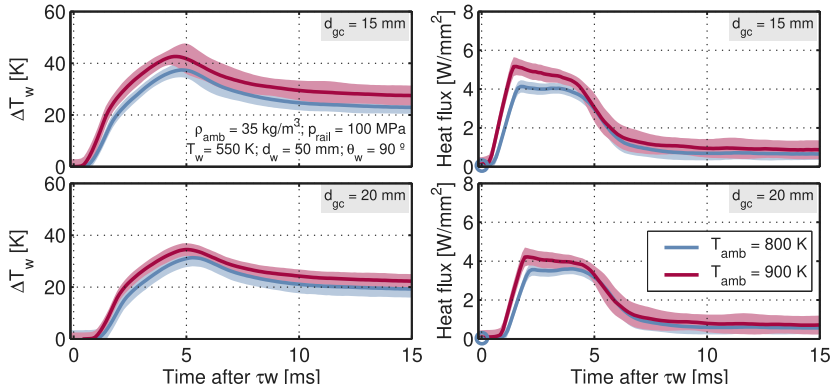

Fig. 31. T_w variation (left) and wall heat flux (right) changing T_{amb} (ρ_{amb} = 35 kg m^{-3}; p_{rail} = 100 MPa; d_w = 50 mm; θ_w = 90°; T_{amb} = 550 K).

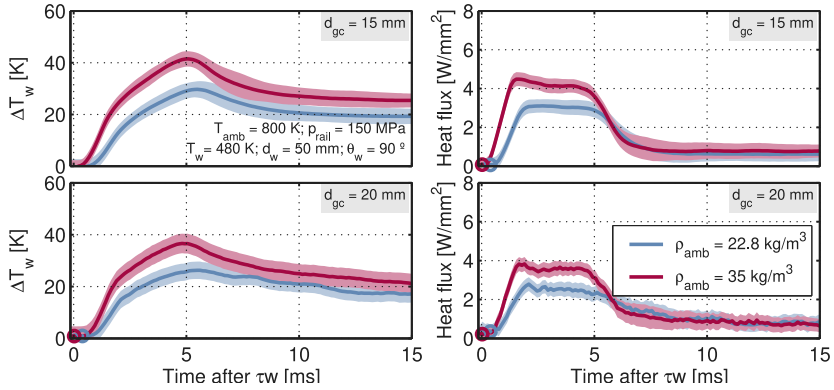

Fig. 32. T_w variation (left) and wall heat flux (right) changing ρ_{amb} (T_{amb} = 800 K; p_{rail} = 150 MPa; d_w = 50 mm; θ_w = 90°; T_w = 480 K).

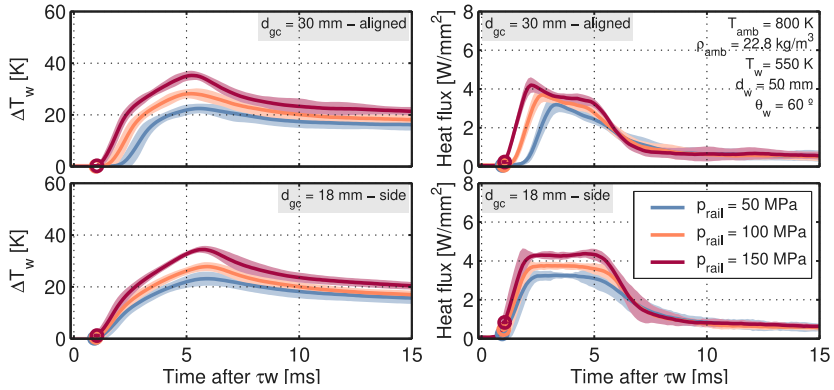

Fig. 33. T_w variation (left) and wall heat flux (right) changing p_{rail} (T_{amb} = 800 K; ρ_{amb} = 22.8 kg m^{-3}; d_w = 50 mm; θ_w = 60°; T_w = 550 K).

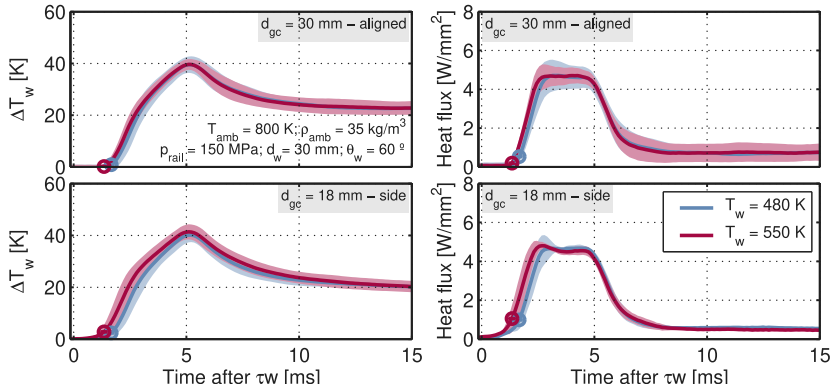

Fig. 34. T_w variation (left) and wall heat flux (right) changing T_w (T_{amb} = 800 K; ρ_{amb} = 35 kg m^{-3}; p_{rail} = 150 MPa; d_w = 30 mm; θ_w = 60°).

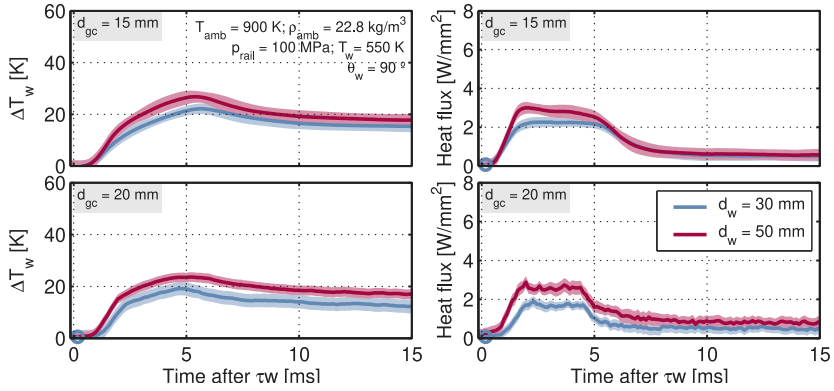

Fig. 35. T_w variation (left) and wall heat flux (right) changing d_w (T_{amb} = 900 K; ρ_{amb} = 22.8 kg m^{-3}; p_{rail} = 100 MPa; θ_w = 90°; T_w = 550 K).

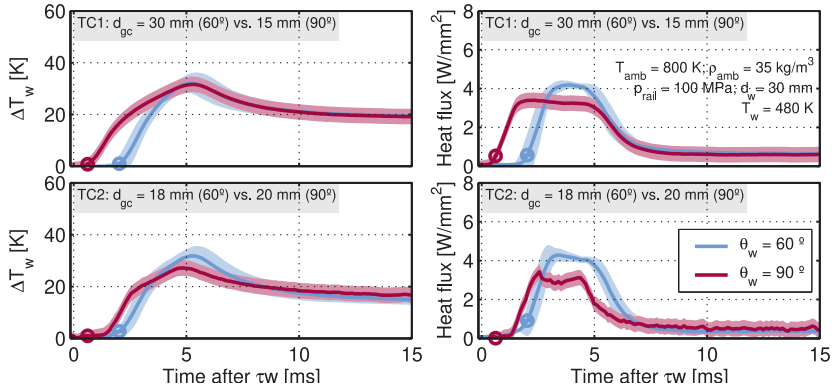

Fig. 36. T_w variation (left) and wall heat flux (right) changing θ_w (T_{amb} = 800 K; ρ_{amb} = 35 kg m^{-3}; p_{rail} = 100 MPa; d_w = 30 mm; T_w = 480 K).

slows down the spray and diminishes the spray–wall exposition, producing a shortening on the ignition delay . Something similar happens with the wall distance, which if it is reduced implies that the spray is cooled down sooner. A boundary layer due to thermal diffusion was formed onto the wall and it gets thicker for the inclined wall, which contributes to cool down the spray and to consequently delay the high temperature chemical reactions. Concerning the geometrical evolution of the spray, its behavior is not different from what was observed from a reacting SWI situation: the spray behaves as an inert spray with the additional influence of the ignition delay in terms of timing and intensity of expansion, which is more intense for more premixed combustion conditions.

- The higher the injection pressure, the higher the spray velocity at the nozzle outlet and the spray momentum flux during both free spray phase and SWI. A higher density promotes the gas entrainment into the spray, making its spreading slower.
- Flame thickness was measured by visualizing soot natural chemiluminescence. It was observed that there is a notable narrowing of the flame with lower wall temperatures, which also affects the profile of the flame thickness respect to a wall at ambient temperature conditions. The 60° wall prevents flame thickness to grow respect to the perpendicular plate due to the aforementioned boundary layer which becomes thicker for the inclined wall.
- Lift-off length was laterally observed with an intensified camera. It was found that the wall temperature in the range of TRI-Wall target conditions did not affect *LoL* location. On the other side, short lift-off lengths remained unaffected by the hardware while the large ones showed to be even larger due to the different effective temperature of the air-fuel mixture from determined zone close to the wall. By increasing the air density and temperature a shortening on the Lift-off length was obtained.
- The transient heat flux transfer by an impinging diesel flame was measured with high temporal resolution. The observed results showed a substantial increment of the heat flux and the wall temperature variation with both ambient temperature and density by increasing the flame temperature and the gas entrainment. An increase in the injection pressure produce an increment in the convective coefficient by changing the mixture-flame velocity and turbulence. The effect of spreading velocity was also observed when the wall angle is changed. The duration from the start of the quasi-steady heat flux to the flame extinction is quite similar for both ambient gas temperatures.

5. Future works

There are many paths that can be followed to continue the work presented in this manuscript, taking into account the relevance of this topic for powertrain research. Below is listed a series of potential possibilities for future developments that can be performed to assess fruitful conclusions beyond the obtained ones from this work:

- The further study of SWI with the liquid phase of the spray could include the use of the thermo-controlled wall in order to analyze the effect of wall temperature on liquid fuel spreading and the wall-cooling capacity of the spray after exchanging energy with the surrounding, by means of the heat flux measuring procedure. Varying energizing times to characterize injection duration effect on SWI or even taking into account multiple-injection strategies, where each injection may change the initial wall conditions in

terms of temperature and deposition formation with respect to the previous ones, is an interesting subject of study.

- Droplet–wall and droplet–droplet collision experiments would be a proper addition to the studies with a tempered wall, as a fundamental approach using techniques such as backlit or PDA measurements. On the other hand, the fuel film formed onto the wall after SWI has been found by researchers to drive unburned hydrocarbons formation, therefore, characterization of post-impingement parameters such as surface wetness, film thickness and distribution at different conditions can be a good addition to this work.
- The employment of a high-speed intensified camera to visualize temporal OH* chemiluminescence would provide not only the evolution of lift-off length, but simultaneous measurements of ignition delay and ignition start location with a single camera and a simpler optical setup. Moreover, experiments with laser-based techniques such as PLIF (Planar Laser-Induced Fluorescence), could be suitable for non-axisymmetrical spray arrangements and it could prevent an optical obstruction of the spray by itself that limit the observation of characteristics such as the thickness profile or long lift-off lengths in SWI situations. Furthermore, soot formation measurements during SWI can be performed in axisymmetrical cases of perpendicular walls or developing techniques to calculate it in inclined impingement conditions.
- The heat flux through the inclined cooled wall showed to be affected by the formation of a convection-driven density gradient layer. Since this region seems to be defined by the cold air that remains on the wall due to gravity, the study of the influence of the wall orientation (same wall turned upside down or rotated 90° in the thermowell axis) on the formation of that layer, and the spray–wall heat flux remains open.
- Major hardware modifications could give place to more potential experiments. From this thesis, the following step to realistic experiments is to implement a bowl-shaped wall for both transparent and tempered plates. This supposes a challenge for both optical access through the wall and its cooling respectively. A single-hole injector was the one used in this thesis. However, jet–jet interaction created on the piston wall after spray spreading is a realistic situation which is really scarce in literature. A radial wall or non-conventional nozzle geometries can be a starting point to conceive this type of campaigns in a similar facility.

Declaration of competing interest

One or more of the authors of this paper have disclosed potential or pertinent conflicts of interest, which may include receipt of payment, either direct or indirect, institutional support, or association with an entity in the biomedical field which may be perceived to have potential conflict of interest with this work. For full disclosure statements refer to https://doi.org/10.1016/j.applthermaleng.2022.118167. Jaime Gimeno reports financial support was provided by Caterpillar Inc. Raul Payri reports financial support was provided by Caterpillar Inc. Jesus E. Peraza reports financial support was provided by Caterpillar Inc.

Acknowledgments

Authors would like to acknowledge Caterpillar Inc. for its support and interest in this work.

The author C. Carvallo thanks the Universitat Politècnica de València for his predoctoral contract (FPI-2019-S1) which is included within the framework of Programa de Apoyo para la Investigación *y* Desarrollo (PAID-01-19).

Finally, the collaboration of Omar Huerta Cornejo and Sergi Soro in the laboratory work and the setup of the hardware is greatly thanked.

References

[1] A.L. Kastengren, F.Z. Tilocco, C.F. Powell, J. Manin, L.M. Pickett, R. Payri, T. Bazyn, Engine combustion network (ECN): Measurements of nozzle geometry and hydraulic behavior, Atom. Sprays 22 (12) (2012) 1011–1052, http://dx.doi.org/10.1615/AtomizSpr.2013006309.

[2] L. Allocca, M. Lazzaro, G. Meccariello, A. Montanaro, Schlieren visualization of a GDI spray impacting on a heated wall: Non-vaporizing and vaporizing evolutions, Energy 108 (2016) 93–98, http://dx.doi.org/10.1016/j.energy.2015.09.107.

[3] R. Payri, J. Gimeno, P. Martí-Aldaraví, A. Viera, Measurements of the mass allocation for multiple injection strategies using the rate of injection and momentum flux signals, Int. J. Engine Res. 22 (4) (2021) 1180–1195, http://dx.doi.org/10.1177/1468087419894854.

[4] C. Tropea, M. Marengo, The impact of drops on walls and films, Multiphase Sci Technol 11 (1998) 11–36, http://dx.doi.org/10.1615/MultScienTechn.v11.i1.20.

[5] S.Y. Lee, S.U. Ryu, Recent progress of spray-wall interaction research, J. Mech. Sci. Technol. 20 (8) (2006) 1101–1117, http://dx.doi.org/10.1007/BF02916010.

[6] A. Montanaro, M. Migliaccio, L. Allocca, V. Fraioli, S.-y. Lee, A. Zhang, J.D. Naber, Schlieren and Mie Scattering Visualization for Single- Hole Diesel Injector under Vaporizing Conditions with Numerical Validation, SAE Technical Paper, 2014, http://dx.doi.org/10.4271/2014-01-1406.

[7] M.R.O. Panão, A.L.N. Moreira, Experimental study of the flow regimes resulting from the impact of an intermittent gasoline spray, Exp. Fluids 37 (2004) 834–855, http://dx.doi.org/10.1007/s00348-004-0868-1.

[8] A.S. Moita, M.R.O. Panão, A.L.N. Moreira, A.S. Moita, M.R.O. Panão, Advances and challenges in explaining fuel spray impingement : How much of single droplet impact research is useful ? Prog. Energy Combust. Sci. 36 (2010) 554–580, http://dx.doi.org/10.1016/j.pecs.2010.01.002.

[9] J.D. Naber, R.D. Reitz, Modeling Engine Spray/Wall Impingement, SAE Technical Paper 880107, 1988, http://dx.doi.org/10.4271/880107.

[10] L. Montorsi, A. Magnusson, S. Andersson, A Numerical and Experimental Study of Diesel Fuel Sprays Impinging on a Temperature Controlled Wall, SAE Technical Paper 2006-01-3333, 2006, pp. 776–790, http://dx.doi.org/10.4271/2006-01-3333.

[11] M. Jia, Z. Peng, M. Xie, R. Stobart, Evaluation of Spray/wall Interaction Models Under the Conditions Related to Diesel HCCI Engines, SAE Technical Paper 1, 2008, pp. 993–1008, http://dx.doi.org/10.4271/2008-01-1632.

[12] H. Yu, X. Liang, G.-Q. Shu, Y. Wang, H. Zhang, W. Chen, Numerical Investigation of the Effect of Alcohol-Diesel Blending Fuels on the Spray-Wall Impingement Process, SAE Technical Papers 2016-April, 2016, http://dx.doi.org/10.4271/2016-01-1276.

[13] F.R. Westlye, M. Battistoni, S.A. Skeen, J. Manin, L.M. Pickett, A. Ivarsson, Penetration and Combustion Characterization of Cavitating and Non-Cavitating Fuel Injectors Under Diesel Engine Conditions, SAE Technical Paper 2016-01-0860, 2016, p. 15, http://dx.doi.org/10.4271/2016-01-0860.

[14] R. Payri, F.J. Salvador, P. Marti-Aldaravi, D. Vaquerizo, ECN spray G external spray visualization and spray collapse description through penetration and morphology analysis, Appl. Therm. Eng. 112 (2017) 304–316, http://dx.doi.org/10.1016/j.applthermaleng.2016.10.023.

[15] J. Gimeno, P. Martí-Aldaraví, M. Carreres, J.E. Peraza, Effect of the nozzle holder on injected fuel temperature for experimental test rigs and its influence on diesel sprays, Int. J. Engine Res. 19 (3) (2018) 374–389, http://dx.doi.org/10.1177/1468087417751531.

[16] J.E. Dec, E.B. Coy, OH radical imaging in a DI diesel engine and the structure of the early diffusion flame, (412) 1996, http://dx.doi.org/10.4271/960831.

[17] M. Bardi, Partial Needle Lift and Injection Rate Shape Effect on the Formation and Combustion of the Diesel Spray (Ph.D. thesis), Universitat Politècnica de València, Valencia (Spain), 2014, http://dx.doi.org/10.4995/Thesis/10251/37374.

[18] J.E. Dec, A Conceptual Model of DI Diesel Combustion Based on Laser-Sheet Imaging, SAE Technical Paper 970873, 1997, http://dx.doi.org/10.4271/970873.

[19] R. Payri, J.M. Garcia-Oliver, M. Bardi, J. Manin, Fuel temperature influence on diesel sprays in inert and reacting conditions, Appl. Therm. Eng. 35 (March) (2012) 185–195, http://dx.doi.org/10.1016/j.applthermaleng.2011.10.027.

[20] R. Payri, J.P. Viera, V. Gopalakrishnan, P.G. Szymkowicz, The effect of nozzle geometry over ignition delay and flame lift-off of reacting direct-injection sprays for three different fuels, Fuel 199 (2017) 76–90, http://dx.doi.org/10.1016/j.fuel.2017.02.075.

[21] R.P. Fitzgerald, K. Svensson, G. Martin, Y. Qi, C. Koci, Early Investigation of Ducted Fuel Injection for Reducing Soot in Mixing-Controlled Diesel Flames, SAE Technical Paper 2018-01-0238, 2018, pp. 1–17, http://dx.doi.org/10.4271/2018-01-0238.

[22] J. Benajes, R. Payri, M. Bardi, P. Martí-aldaraví, Experimental characterization of diesel ignition and lift-off length using a single-hole ECN injector, Appl. Therm. Eng. 58 (1–2) (2013) 554–563, http://dx.doi.org/10.1016/j.applthermaleng.2013.04.044.

[23] R. Payri, F.J. Salvador, J. Manin, A. Viera, Diesel ignition delay and lift-off length through different methodologies using a multi-hole injector, Appl. Energy 162 (2016) 541–550, http://dx.doi.org/10.1016/j.apenergy.2015.10.118.

[24] N. Peters, Turbulent Combustion, in: Cambridge Monographs on Mechanics, Cambridge University Press, 2000, http://dx.doi.org/10.1017/CBO9780511612701.

[25] P.C. Miles, O. Andersson, A review of design considerations for light-duty diesel combustion systems, Int. J. Engine Res. 17 (1) (2016) 6–15, http://dx.doi.org/10.1177/1468087415604754.

[26] L. XiangRong, Z. WeiHua, G. HaoBu, L. FuShui, Fuel and air mixing characteristics of wall-flow-guided combustion systems under a low excess air ratio condition in direct injection diesel engines, Energy 175 (2019) 554–566, http://dx.doi.org/10.1016/J.ENERGY.2019.03.120.

[27] F. Perini, K. Zha, S. Busch, E. Kurtz, R.C. Peterson, A. Warey, R.D. Reitz, Piston geometry effects in a light-duty, swirl-supported diesel engine: Flow structure characterization, Int. J. Engine Res. 19 (10) (2018) 1079–1098, http://dx.doi.org/10.1177/1468087417742572.

[28] X. Wang, Z. Huang, W. Zhang, O.A. Kuti, K. Nishida, Effects of ultra-high injection pressure and micro-hole nozzle on flame structure and soot formation of impinging diesel spray, Appl. Energy 88 (5) (2011) 1620–1628, http://dx.doi.org/10.1016/j.apenergy.2010.11.035.

[29] L.M. Pickett, J.J. Lopez, Jet-wall interaction effects on diesel combustion and soot formation 2005, 2005.

[30] R. Payri, J.P. Viera, V. Gopalakrishnan, P.G. Szymkowicz, The effect of nozzle geometry over internal flow and spray formation for three different fuels, Fuel 183 (2016) 20–33, http://dx.doi.org/10.1016/j.fuel.2016.06.041.

[31] R. Payri, J. Gimeno, G. Bracho, D. Vaquerizo, Study of liquid and vapor phase behavior on diesel sprays for heavy duty engine nozzles, Appl. Therm. Eng. 107 (2016) 365–378, http://dx.doi.org/10.1016/j.applthermaleng.2016.06.159.

[32] ECN, Engine combustion network, 2010, URL: www.sandia.gov/ecn/.

[33] J. Manin, L.M. Pickett, K. Yasutomi, Transient cavitation in transparent diesel injectors, in: ICLASS 14th Triennial International Conference on Liquid Atomization and Spray Systems, Chicago, 2018, pp. 1–9.

[34] K. Yasutomi, J. Hwang, L.M. Pickett, B. Sforzo, K. Matusik, C.F. Powell, Transient Internal Nozzle Flow in Transparent Multi-Hole Diesel Injector, SAE Technical Papers, 2020, pp. 1–13, http://dx.doi.org/10.4271/2020-01-0830.

[35] M. Battistoni, G.M. Magnotti, C.L. Genzale, M. Arienti, K.E. Matusik, D.J. Duke, J. Giraldo, J. Ilavsky, A.L. Kastengren, C.F. Powell, P. Marti-Aldaravi, Experimental and Computational Investigation of Subcritical Near-Nozzle Spray Structure and Primary Atomization in the Engine Combustion Network Spray D, SAE Technical Paper, 2018, pp. 1–15, http://dx.doi.org/10.4271/2018-01-0277.

[36] R. Payri, J. Gimeno, S. Cardona, S. Ayyapureddi, Experimental study of the influence of the fuel and boundary conditions over the soot formation in multi-hole diesel injectors using high-speed color diffused back-illumination technique, Appl. Therm. Eng. 158 (2019) 113746, http://dx.doi.org/10.1016/J.APPLTHERMALENG.2019.113746.

[37] R. Payri, J. Gimeno, S. Cardona, S. Ayyapureddi, Measurement of Soot Concentration in a Prototype Multi- Hole Diesel Injector by High-Speed Color Diffused Back Illumination Technique, SAE Technical Paper 2017-01-2255, 2017, http://dx.doi.org/10.4271/2017-01-2255.

[38] C. Gong, M. Jangi, X.S. Bai, Large eddy simulation of n-dodecane spray combustion in a high pressure combustion vessel, Appl. Energy 136 (2014) 373–381, http://dx.doi.org/10.1016/j.apenergy.2014.09.030.

[39] L.M. Pickett, C.L. Genzale, J. Manin, Uncertainty quantification for liquid penetration of evaporating sprays at diesel-like conditions, Atom. Sprays 25 (5) (2015) 425–452, http://dx.doi.org/10.1615/AtomizSpr.2015010618.

[40] J.M. Desantes, R. Payri, F.J. Salvador, A. Gil, Development and validation of a theoretical model for diesel spray penetration, Fuel 85 (7–8) (2006) 910–917, http://dx.doi.org/10.1016/j.fuel.2005.10.023.

[41] J.D. Naber, D.L. Siebers, Effects of Gas Density and Vaporization on Penetration and Dispersion of Diesel Sprays, SAE Paper 960034, Society of Automotive Engineers, Inc., Warrendale, Pennsylvania, USA, 1996, http://dx.doi.org/10.4271/960034.

[42] J. Gimeno, G. Bracho, P. Martí-Aldaraví, J.E. Peraza, Experimental study of the injection conditions influence over n-dodecane and diesel sprays with two ECN single-hole nozzles. Part I: Inert atmosphere, Energy Convers. Manage. 126 (2016) 1146–1156, http://dx.doi.org/10.1016/j.enconman.2016.07.077.

[43] B. Chen, L. Feng, Y. Wang, T. Ma, H. Liu, C. Geng, M. Yao, Spray and flame characteristics of wall-impinging diesel fuel spray at different wall temperatures and ambient pressures in a constant volume combustion vessel, Fuel 235 (March 2018) (2019) 416–425, http://dx.doi.org/10.1016/j.fuel.2018.07.154.

[44] J.E. Peraza, R. Payri, J. Gimeno, P.M. Aldaraví, ECN spray D visualization of the spray interaction with a transparent wall under engine-like conditions. Part II: Impinging spray combustion, Fuel 308 (2022) 121964, http://dx.doi.org/10.1016/j.fuel.2021.121964.

[45] R. Payri, J. Gimeno, J.E. Peraza, T. Bazyn, Spray / wall interaction analysis on an ECN single-hole injector at diesel-like conditions through schlieren visualization, in: Proc. 28th ILASS-Europe, Valencia, 2017, http://dx.doi.org/10.4995/ILASS2017.2017.4709.

[46] R. Payri, J.M. Garcia-Oliver, T. Xuan, M. Bardi, A study on diesel spray tip penetration and radial expansion under reacting conditions, Appl. Therm. Eng. 90 (2015) 619–629, http://dx.doi.org/10.1016/j.applthermaleng.2015.07.042.

[47] R. Payri, F.J. Salvador, J. Gimeno, J.E. Peraza, Experimental study of the injection conditions influence over n-dodecane and diesel sprays with two ECN single-hole nozzles. Part II: Reactive atmosphere, Energy Convers. Manage. 126 (2016) 1157–1167, http://dx.doi.org/10.1016/j.enconman.2016.07.079.

[48] A.N. Lipatnikov, W.Y. Li, L.J. Jiang, S.S. Shy, Does density ratio significantly affect turbulent flame speed? Flow Turbul. Combust. 98 (4) (2017) 1153–1172, http://dx.doi.org/10.1007/s10494-017-9801-6.

[49] W. Du, Q. Zhang, Z. Zhang, J. Lou, W. Bao, Effects of injection pressure on ignition and combustion characteristics of impinging diesel spray, Appl. Energy 226 (February) (2018) 1163–1168, http://dx.doi.org/10.1016/j.apenergy.2018.06.032.

[50] N. Maes, M. Hooglugt, N. Dam, B. Somers, G. Hardy, On the influence of wall distance and geometry for high-pressure n-dodecane spray flames in a constant-volume chamber, Int. J. Engine Res. (2019) http://dx.doi.org/10.1177/1468087419875242.

[51] A.M. Rusly, M.K. Le, S. Kook, E.R. Hawkes, The shortening of lift-off length associated with jet-wall and jet-jet interaction in a small-bore optical diesel engine, Fuel 125 (2014) 1–14, http://dx.doi.org/10.1016/j.fuel.2014.02.004.

[52] A. Magnusson, S. Andersson, S. Jedrzejowski, Spray-Wall Interaction: Diesel Fuels Impinging on a Tempered Wall, SAE Technical Paper 2006-01-1116, 2006, http://dx.doi.org/10.4271/2006-01-1116.

[53] J. Moussou, G. Pilla, F. Rabeau, J. Sotton, M. Bellenoue, High-frequency wall heat flux measurement during wall impingement of a diffusion flame, Int. J. Engine Res. (2019) http://dx.doi.org/10.1177/1468087419878040.

[54] Z. Zhao, X. Zhu, L. Zhao, J. Naber, S.-Y. Lee, Spray-wall dynamics of high-pressure impinging combustion, 2019, http://dx.doi.org/10.4271/2019-01-0067.

[55] R. Mahmud, S.B. Kim, T. Kurisu, K. Nishida, Y. Ogata, J. Kanzaki, T. Tadokoro, Characteristics of Flat-Wall Impinging Spray Flame and its Heat Transfer under Small Diesel Engine-Like Condition, SAE Technical Paper 2017-32-0032, 2017.

[56] Y. Jiotode, A. Agarwal, Endoscopic combustion characterization of jatropha biodiesel in a compression ignition engine, Energy 119 (2016) http://dx.doi.org/10.1016/j.energy.2016.11.056.

[57] G. Mao, K. Shi, C. Zhang, S. Chen, P. Wang, Experimental research on effects of biodiesel fuel combustion flame temperature on NOX formation based on endoscope high-speed photography, J. Energy Inst. (X) (2020) 1–12, http://dx.doi.org/10.1016/j.joei.2020.01.002.

[58] S.K. Jha, S. Fernando, S.D. To, Flame temperature analysis of biodiesel blends and components, Fuel 87 (10–11) (2008) 1982–1988, http://dx.doi.org/10.1016/j.fuel.2007.10.026.

[59] P. Flynn, R.P. Durrett, G. Hunter, A. ZurLoye, O.C. Akinyemi, J.E. Dec, C. Westbrook, Diesel Combustion: an Integrated View Combining Laser Diagnostics, Chemical Kinetics, and Empirical Validation, SAE Paper 1999-01-0509, 1999.

[60] G. Bruneaux, Combustion structure of free and wall-impinging diesel jets by simultaneous laser-induced fluorescence of formaldehyde, poly-aromatic hydrocarbons, and hydroxides, Int. J. Engine Res. 9 (3) (2008) 249–265, http://dx.doi.org/10.1243/14680874JER00108.

[61] T. Ma, L. Feng, H. Wang, H. Liu, M. Yao, Analysis of near wall combustion and pollutant migration after spray impingement, Int. J. Heat Mass Transfer 141 (2019) 569–579, http://dx.doi.org/10.1016/j.ijheatmasstransfer.2019.07.001.